

ELVIS: Exploring the Local Volume in Simulations

Shea Garrison-Kimmel^{1*}, Michael Boylan-Kolchin^{2,1}, James S. Bullock¹, Kyle Lee³

¹*Center for Cosmology, Department of Physics and Astronomy, University of California, Irvine, CA 92697, USA*

²*Department of Astronomy and Joint Space-Science Institute, University of Maryland, College Park, MD 20742-2421, USA*

³*Chapman University, Orange, CA 92866, USA*

3 December 2024

ABSTRACT

We introduce a set of high-resolution dissipationless simulations that model the Local Group (LG) in a cosmological context: Exploring the Local Volume in Simulations (ELVIS). The suite contains 48 galaxy-size halos, each within high-resolution volumes that span 2–5 Mpc in size, and each resolving thousands of systems with masses below the atomic cooling limit. Half of the ELVIS galaxy halos are in paired configurations similar to the Milky Way (MW) and M31; the other half are isolated, mass-matched analogs. We find no difference in the abundance or kinematics of substructure within the virial radii of isolated versus paired hosts. On Mpc scales, however, LG-like pairs average almost twice as many companions and the velocity field is kinematically hotter and more complex. We present a refined abundance matching relation between stellar mass and halo mass that reproduces the observed satellite stellar mass functions of the MW and M31 down to the regime where incompleteness is an issue, $M_* \sim 5 \times 10^5 M_\odot$. Within a larger region spanning approximately 3 Mpc, the same relation predicts that there should be ~ 1000 galaxies with $M_* > 10^3 M_\odot$ awaiting discovery. We show that up to 50% of halos within 1 Mpc of the MW or M31 could be systems that have previously been within the virial radius of either giant. By associating never-accreted halos with gas-rich dwarfs, we show that there are plausibly 50 undiscovered dwarf galaxies with HI masses $> 10^5 M_\odot$ within the Local Volume. The radial velocity distribution of these predicted gas-rich dwarfs can be used to inform follow-up searches based on ultra-compact high-velocity clouds found in the ALFALFA survey.

Key words: dark matter – cosmology: theory – galaxies: haloes – Local Group

1 INTRODUCTION

The Local Group (LG) provides an important test bed for theories of galaxy formation, both in its connection to small-scale probes of the consensus dark energy plus cold dark matter (Λ CDM) cosmological model (Klypin et al. 1999; Moore et al. 1999; Strigari et al. 2008; Walker & Peñarrubia 2011; Boylan-Kolchin et al. 2011; Zolotov et al. 2012; Garrison-Kimmel et al. 2013; Arraki et al. 2012) and as a potential hunting ground for the descendants of reionization and first light (Bullock et al. 2000; Ricotti & Gnedin 2005; Madau et al. 2008). The focus on these issues is well-motivated: given inevitable completeness limitations, nearby galaxies offer our best avenue for characterizing the faint end of the global luminosity function and for studying resolved stellar populations as beacons from an earlier age (see, e.g. Makarov & Karachentsev 2011; Weisz et al. 2011; McConnachie 2012; Karachentsev & Kaisina 2013; Tully et al. 2013).

Numerical simulations have emerged as the most useful tool for making predictions about non-linear structures in Λ CDM. While simulations of cosmologically large volumes enable statistical comparisons with a variety of observations (e.g. Davis et al. 1985; Gross et al. 1998; Springel et al. 2005; Boylan-Kolchin et al. 2009; Klypin et al. 2011), cosmological zoom-in simulations are the de facto standard for the most detailed comparisons of individual objects. The zoom-in technique (Katz & White 1993; Oñorbe et al. 2013) focuses computational power on a small, high resolution region nested within a lower resolution, cosmological-size volume, thereby retaining the large-scale, low frequency cosmological modes important for convergence but also allowing for the high resolutions required to obtain a wide dynamic range.

Very high resolution zoom-in simulations of Milky Way-mass halos have been useful for making and testing predictions of the Λ CDM theory (e.g. Diemand et al. 2008; Kuhlen et al. 2008; Springel et al. 2008), often through comparisons to dwarf satellite galaxies of the Local Group (Koposov et al. 2009; Strigari et al. 2010; Boylan-Kolchin et al. 2012). However, in order to achieve the highest resolution possible, these

* sgarriso@uci.edu

simulations have concentrated on fairly isolated systems.¹ In reality, the Milky Way is not isolated, but has a nearby companion of comparable luminosity, the Andromeda galaxy (M31). The existence of M31 at a distance of approximately 800 kpc from the MW implies that isolated zoom simulations cannot be used to faithfully make predictions for the Local Volume² beyond ~ 400 kpc of either system. Furthermore, several simulations that have explored the role of Local-Group like environments in shaping galaxy properties have found evidence that the local configuration may even bias galaxy properties within each giant’s virial radius compared to isolated counterparts (Gottloeber et al. 2010; Libeskind et al. 2010; Forero-Romero et al. 2011; Few et al. 2012).

Motivated by these concerns, here we introduce a set of dissipationless simulations designed to confront the Local Volume in a cosmological context. We call this project ELVIS: Exploring the Local Volume in Simulations. The simulation suite consists of twelve zoom-in regions of LG analog halo pairs and twenty-four isolated halos that are mass-matched to create a control sample for those pairs. Below, we describe the selection of ELVIS pairs, their simulation details, and properties of the host halos (§ 2). We investigate the environments that surround them in comparison to those of the control hosts as well as the dynamical histories of bound halos around the ELVIS giants by characterizing the fraction of “backsplash” halos – systems that at one point had been within the virial radius of a giant – as a function of distance (§ 3). Finally, we compare number counts and kinematic properties of the subhalos found in paired and isolated samples, and we use abundance matching to make predictions for the stellar and HI mass functions within the Local Volume (§ 4).

With the publication of this paper, we will publicly release all of the data in the ELVIS suite, including full merger trees, $z = 0$ halo catalogs, and particle information.³

2 THE ELVIS SUITE

The ELVIS simulations were run using GADGET-3 and GADGET-2 (Springel 2005), both tree-based N -body codes. For the underlying cosmological model, we have adopted Λ CDM parameters set by the WMAP-7 results (Larson et al. 2011): $\sigma_8 = 0.801$, $\Omega_m = 0.266$, $\Omega_\Lambda = 0.734$, $n_s = 0.963$, and $h = 0.71$. Throughout this work, we use the term virial mass M_v to refer to the mass within a sphere of radius R_v that corresponds to an over density of 97 relative to the critical

¹ As noted in Teyssier et al. (2012), the Via Lactea II halo does indeed have a massive ($M_v = 6.5 \times 10^{11} M_\odot$) companion at a distance comparable to M31. However, this companion halo and field galaxies nearby are not free of contamination from low-mass particles. The contamination reaches 50% by mass, which has potentially important effects on halo properties.

² A term we use roughly to correspond to a ~ 2 Mpc sphere from the LG barycenter.

³ Present day ($z = 0$) halo catalogs and the main branches of the merger trees will be made available for public download (<http://localgroup.ps.uci.edu/elvis>), while access to the full merger trees and particle information will be arranged via email contact with the authors.

density of the universe (Bryan & Norman 1998). All simulations were initialized at redshift $z = 125$ unless otherwise specified.

2.1 Halo Selection

We select LG-like pairs from fifty medium-resolution cosmological simulations, each a cubic volume 70.4 Mpc on a side with particle mass $m_p = 9.7 \times 10^7 M_\odot$ and Plummer-equivalent force softening length 1.4 kpc (comoving). From these cosmological volumes, we selected twelve halo pairs for resimulation using the criteria described below. For each of the twenty-four halos included in the ELVIS pairs, we also chose an isolated analog of identical virial mass (M_v) that is separated by at least 2.8 Mpc from all halos more massive than $M_v/2$. The isolated set serves as a control sample for comparison.

Our approach to selecting LG regions differs from that of the well-known CLUES project (Gottloeber et al. 2010), which relies on the “constrained realization” technique to match the observed density and velocity fields on a ~ 10 Mpc scales around the Local Group. The advantage to our approach is that it guarantees a good Local Group analog in each re-simulation. The downside is that the larger scale density field will usually not be identical to that of the Local Group. The two initialization methods therefore have different, complementary strengths.

In selecting pairs, we targeted halos with phase-space characteristics similar to the MW/M31 system, with cuts similar to those of Forero-Romero et al. (2011), based on values of the virial mass of each host ($M_{v,1}$ and $M_{v,2}$, where $M_{v,2} \geq M_{v,1}$), the distance between host centers ΔR , the pair approach velocity, and local environment:

- *Mass of each host:* $10^{12} \leq M_v \leq 3 \times 10^{12} M_\odot$
(Tollerud et al. 2012; Boylan-Kolchin et al. 2013; Fardal et al. 2013; Piffl et al. 2013)
- *Total mass:* $2 \times 10^{12} \leq M_{v,1} + M_{v,2} \leq 5 \times 10^{12} M_\odot$
(Li & White 2008; van der Marel et al. 2012)
- *Separation:* $0.6 \leq \Delta R \leq 1$ Mpc
(McConnachie et al. 2005, and references therein)
- *Radial velocity:* $V_{\text{rad}} \leq 0$ km/s
(van der Marel et al. 2012)
- *Isolation:* No halos with $M_v \geq M_{v,1}$ within 2.8 Mpc of either center and no halos with $M_v \geq 7 \times 10^{13} M_\odot$ within 7 Mpc of either center (Tikhonov & Klypin 2009; Karachentsev et al. 2004).

We identified 146 halo pairs that met these criteria within the fifty simulations we ran (an equivalent volume of 1.76×10^7 Mpc³) and selected twelve pairs for resimulation. We intentionally chose several pairs that consisted of hosts with massive ($V_{\text{max}} > 75$ km s⁻¹) subhalos in order to ensure that we had a fair number of systems with realistic analogs to the LMC and M33; had we selected pairs at random, it would have been unlikely to obtain such massive subhalos (Boylan-Kolchin et al. 2010). We further made an effort to include two pairs that had very low relative tangential velocities < 15 km s⁻¹ in order to mimic the low rel-

ative tangential speed of the MW/M31 pair (van der Marel et al. 2012). For the isolated control sample, we imposed no selection choices other than in matching virial masses and demanding that there are no halos with $M > M_v/2$ within 2.8 Mpc. Most of the matches in mass are good to within 5%, though some differ by up to 10%. Though we attempted to match their masses at the percent level in the low-resolution simulations used to identify objects for resimulation, differences of this order are expected when using the zoom-in technique (Oñorbe et al. 2013).

For record-keeping purposes, each LG-analog pair is named after a famous duo, as summarized in Table 1. The individual halos that make up the pairs are referenced by the same names in Table 2. The isolated analogs are identified by the same name prefixed by i in Table 3. We discuss the information presented in these tables in Section 2.3. The first pair listed in Table 1, Zeus & Hera, is singled-out in several figures below as a good analog to the M31/MW system in terms of observed galaxy counts in the Local Volume region. The halo Hera is identified with the Milky Way in this pairing.

2.2 Zoom Simulations

In creating the zoom-in initial conditions for the ELVIS halos, we broadly followed the methods outlined in Oñorbe et al. (2013), who give prescriptions for selecting regions that will be free from low-resolution particle contamination in the final run. For the pairs, we identified Lagrangian volumes for all particles within $4 R_v$ of either host in the final timestep; for the isolated analogs, we use particles within $5 R_v$ in all but one case (specified below). We relied on the public⁴ code MUSIC (Hahn & Abel 2011) to create initial conditions associated with these Lagrangian volumes at high resolution. The mass resolution in the zoom regions of our production runs is $m_p = 1.9 \times 10^5 M_\odot$, corresponding to an effective resolution of 4096^3 in the box. The Plummer-equivalent force softening, ϵ , in these runs was held constant in comoving units until $z = 9$, at which point it was held fixed at 141 pc (physical) for the remainder of each simulation.

The high resolution regions are surrounded by stepped levels of progressively lower force resolution and higher mass particles, with the majority of the parent boxes (70.4 Mpc cubes) filled with an effective resolution of 128^3 ($m_p = 6.2 \times 10^9 M_\odot$) and each successive step increasing the effective resolution by a factor of 2 (decreasing the particle mass by a factor of 8). As in the high resolution regions, ϵ remains constant in comoving units until $z = 9$, then becomes fixed in physical units. These force softenings, however, are significantly larger than in the high resolution regions: at $z = 0$ in the main runs, the two highest particle masses utilize $\epsilon = 56$ kpc, the two intermediate regions use $\epsilon = 4.2$ kpc, and $\epsilon = 704$ pc for the particles immediately surrounding the high resolution volume.

Self-bound dark matter clumps are identified with the six-dimensional halo finder Rockstar (Behroozi et al. 2013a) and followed through cosmic time with consistent-trees (Behroozi et al. 2013b). Both of these codes are publicly

available.⁵ Subhalo masses (M) are calculated by Rockstar and correspond to the bound mass of the system. Maximum circular velocities (V_{\max}) correspond to the peak of the circular velocity curve, $V_c(r) = \sqrt{GM(r)/r}$, at a given redshift. We also checked results at the final timestep ($z = 0$) against the public⁶, spherical overdensity-based Amiga Halo Finder (Knollmann & Knebe 2009) and found that the results did not differ significantly and were identical within the statistical variation of our sample of halos.⁷

Three of the most useful quantities that can be determined for halos in our simulations are M_{peak} (the maximum mass of a dark matter structure over its history), a_{peak} (the latest scale factor at which M_{peak} occurs), and V_{peak} (the maximum circular velocity at a_{peak}). To define these quantities, one must adopt an unambiguous definition of the main branch of each halo’s merger tree. We assign the main progenitor at each timestep as the branch of the tree with the most total mass up to and including that timestep, i.e., the sum of M_v for all halos over all preceding timesteps in that branch. This definition weights both the formation time and the virial mass of halos in a given branch. The final step in our pipeline identifies the main branch of each merger tree and extracts M_{peak} , V_{peak} , and a_{peak} for each halo with $z = 0$ quantities M (or M_v for hosts) and V_{\max} .

We simulated three of the isolated analogs (iScylla, iKauket, and iHall) at higher resolution, with $m_p = 2.35 \times 10^4 M_\odot$ (8192^3 effective particle number) and $\epsilon = 70.4$ pc; we refer to these runs as the HiRes simulations. The HiRes version of iKauket was originally simulated in the context of previous work (Oñorbe et al. 2013) and was initialized at a different redshift ($z = 250$) than the rest of our runs. It also used a Lagrangian volume chosen from all particles within $2 R_v$ (rather than our fiducial $5 R_v$ for the other isolated systems). The standard resolution version of iKauket also started at $z = 250$. As Oñorbe et al. (2013) showed, any variation in halo properties introduced by such a change in initial redshift are comparable to expected variations upon resimulation due to numerical “minichaos” (Miller 1964), which should be unimportant for our purposes.

Our HiRes simulations are comparable in mass and force resolution to the Aquarius level 2 simulations (Springel et al. 2008) and to VL-I (Diemand et al. 2007a), though two of them (iScylla and iHall) have uncontaminated high-resolution volumes – uncontaminated spheres of radius ~ 1.5 Mpc around each host – that extend much farther from the halo centers than any previous runs of this kind. The HiRes simulations will facilitate several inquiries that are not possible with our fiducial runs, but for the purposes of this paper, they have allowed us to self-consistently identify the completeness limit for subhalos in our main ELVIS suite. We find that we are complete to $M > 2 \times 10^7 M_\odot$, $V_{\max} > 8 \text{ km s}^{-1}$, $M_{\text{peak}} > 6 \times 10^7 M_\odot$ and $V_{\text{peak}} > 12 \text{ km s}^{-1}$. The numerical convergence of our results in V_{\max} and M_{peak} is demonstrated explicitly for iKauket in Appendix A.

In the bulk of this paper, we will enumerate halos and

⁵ The links are <http://code.google.com/p/rockstar/> and <http://code.google.com/p/consistent-trees/>.

⁶ The link is <http://popia.ft.uam.es/AHF/>

⁷ Though our results presented here and made publicly available upon publication rely on Rockstar, we are happy to supply associated Amiga Halo Finder catalogs upon request.

⁴ The link is <http://www.phys.ethz.ch/~hahn/MUSIC/>

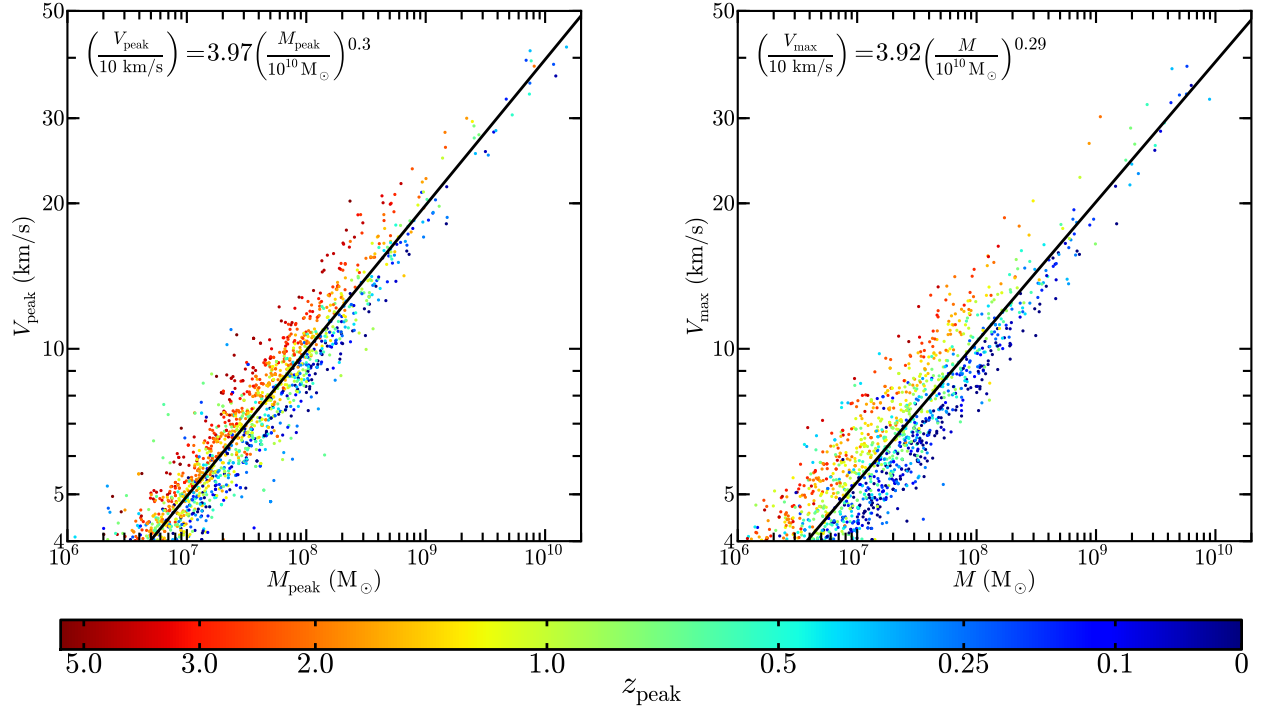


Figure 1. The relation between peak circular velocity and mass at a_{peak} (left) and at $z = 0$ (right). The indicated fit includes all resolved halos within 400 kpc of iKauket in the HiRes run (though the results do not differ at the fiducial resolution). Each subhalo is colored by the redshift at which it reached its peak mass (a_{peak}); this quantity is well-correlated with the scatter about the fits and, as is evident from the right panel, the amount of tidal stripping each subhalo has undergone.

subhalos based on M_{peak} . One could equivalently present results in terms of M , V_{max} , or V_{peak} (V_{max} functions are presented Appendix B). Figure 1 demonstrates the relationship between M_{peak} and V_{peak} (left panel) and M and V_{max} (right panel) for halos within 400 kpc of the HiRes version of iKauket (the results are indistinguishable for the fiducial resolution runs for $V_{\text{max}} > 8 \text{ km s}^{-1}$ and $M_{\text{peak}} > 6 \times 10^7 M_{\odot}$.) The best-fit $M_{\text{peak}} - V_{\text{peak}}$ and $M - V_{\text{max}}$ relations are given by the formulas in the figures themselves.

What is the origin of the scatter in the $V - M$ relations? The points in Figure 1 are colored by $z_{\text{peak}} = a_{\text{peak}}^{-1} - 1$. We see that this variable is strongly correlated with the scatter in V at fixed M , such that earlier-forming halos have higher values of V_{peak} and V_{max} . The correlation between a_{peak} and V_{peak} is related to the redshift dependence of the concentration-mass relation (Bullock et al. 2001), while the correlation between a_{peak} and V_{max} is a combination of the $a_{\text{peak}} - V_{\text{peak}}$ correlation and the effects of orbital evolution on subhalo density structure (for discussions on these expected trends see, e.g., Zentner & Bullock 2003; Kazantzidis et al. 2004; Diemand et al. 2007b).

2.3 General Properties of the ELVIS halos

Table 1 summarizes the names and some properties of the ELVIS pairs at $z = 0$ (along with comparative information for the Milky Way and M31, where appropriate). We include the physical separation between halo centers, their relative

radial and tangential velocities,⁸ as well as their virial masses and virial mass ratios. Column 7 lists a conservative estimate of the high-resolution simulation volume \mathcal{V}_{res} , defined as the union of the two maximal spheres, centered on each pair, that is uncontaminated by any lower resolution particles. Columns 8 and 9 list the overall number of halos (above our completeness limit of $V_{\text{max}} > 8 \text{ km s}^{-1}$) and number of simulation particles contained within the volume \mathcal{V}_{res} . The final column lists the V_{max} value of and distances to the largest halo within 1.2 Mpc of either host (but outside of the 300 kpc virial region), which serve as an indication of the larger-scale environment. Note that the virial volumes of Hera and Zeus slightly overlap; however, only a single subhalo is identified in that overlapping volume, so the effect on subsequent results is negligible.

Two of the pairs – Siegfried & Roy and Serena & Venus – have a particularly large halo ($V_{\text{max}} = 157, 159 \text{ km s}^{-1}$) within 1.2 Mpc of one of the hosts. This may seem contrary to our isolation criteria, but in both cases this third halo is less massive than either of the paired hosts. Nevertheless, the presence of the massive companions may render these pairs less than ideal comparison sets for the real Local Group. In all figures below that make predictions for the overall count of galaxies expected within ~ 1 Mpc scales, we either remove

⁸ The kinematics of our pairs as listed Table 1 are consistent with those found for a larger number of pairs in simulations by Forero-Romero et al. (2013).

Pair Name	ΔR (kpc)	V_{rad} (km/s)	V_{tan} (km/s)	Total Mass ^a ($10^{12}M_{\odot}$)	Mass Ratio ^b	V_{res} ^c (Mpc ³)	N_{halos} ^d ($< V_{\text{res}}$)	N_{p} ^e ($< V_{\text{res}}$)	$[V_3, D_{\ell}, D_s]$ ^f (km/s, Mpc, Mpc)	
Zeus & Hera	595	-158.4	173.6	3.98	2.05	39.7	3,956	44M	[73, 0.73, 1.3]	
Scylla & Charybdis	705	-21.1	132.4	3.97	1.45	38.1	4,381	47M	[105, 0.50, 1.09]	
Romulus & Remus	935	-20.4	13.2	3.15	1.53	34.6	2,522	30M	[62, 0.40, 1.33]	
Orion & Taurus	829	-69.8	62.9	4.04	2.38	24.7	2,856	36M	[56, 1.06, 1.90]	
Kek & Kauket	1040	-32.3	38.6	3.25	2.06	43.2	3,461	40M	[114, 0.96, 1.68]	
Hamilton & Burr	941	-18.0	37.7	3.26	1.17	24.7	2,882	32M	[54, 1.39, 0.57]	
Lincoln & Douglas	780	-86.6	42.4	3.89	1.90	18.2	2,801	33M	[60, 1.86, 1.16]	
Serena & Venus*	687	-109.0	71.0	4.26	1.94	24.9	4,797	55M	[159, 0.89, 1.54]	
Sonny & Cher	966	-104.9	42.0	3.69	1.05	9.7	2,290	29M	[84, 0.99, 0.84]	
Hall & Oates	980	-8.9	43.7	2.71	1.26	14.5	1,713	24M	[64, 1.07, 1.59]	
Thelma & Louise	832	-52.4	11.0	2.36	1.30	5.3	1,693	20M	[64, 1.13, 0.46]	
Siegfried & Roy*	878	-68.5	57.6	4.31	1.02	11.9	5,087	61M	[157, 0.61, 1.09]	
Milky Way & M31	770 ± 80 ^g	-109 ± 9 ^g	< 52 ^g	3.8 ± 0.7 ^h	1.26	$\begin{smallmatrix} +0.69 \\ -0.24 \end{smallmatrix}$ ⁱ	–	–	–	[64, 0.89, 0.45] ^j

^a Sum of virial masses: $M_{v,1} + M_{v,2}$

^b Ratio of virial masses: $M_{v,2}/M_{v,1}$, where $M_{v,2} \geq M_{v,1}$ by definition.

^c Bi-spherical volume of the high resolution region at $z = 0$ that is uncontaminated by low-resolution particles. Specifically, V_{res} is defined as the union of the two maximal spheres, centered on each pair, that are uncontaminated.

^d Number of identified halos with $V_{\text{max}} > 8$ km/s that sit within the high-resolution volume V_{res} .

^e Number of particles in millions (rounded to the nearest million) within the high-resolution volume V_{res} .

^f The value of V_{max} for and distances to the largest halo within 1.2 Mpc of either host that is not within 300 kpc of either host. The distances listed are relative to the larger and smaller of the two hosts, respectively.

^g As given in van der Marel et al. (2012) with $2\text{-}\sigma$ uncertainties quoted.

^h In listing this value, we average the timing argument result $M_{v,1} + M_{v,2} = (4.3 \pm 1.1) \times 10^{12} M_{\odot}$ from van der Marel et al. (2012)

and the sum of our fiducial M_{v}^{MW} and $M_{\text{v}}^{\text{M31}}$ values listed in Table 2. Quoted uncertainties are $2\text{-}\sigma$.

ⁱ The quoted average and ratio takes into account that the quantity is defined to be larger than unity. It combines the constraints listed in Table 2 and quotes 90% uncertainties.

^j We list the most luminous galaxy within 1.2 Mpc of either the MW or M31 according to McConnachie (2012): NGC 6822 with $L_{\text{V}} = 1.04 \times 10^8 L_{\odot}$ and $M_{*} = 8.3 \times 10^7 M_{\odot}$. We let $D_{\ell} = D_{\text{M31}}$ and $D_s = D_{\text{MW}}$. The V_{max} listed for NGC 6822 is very rough, and is based on assuming the abundance matching prescription described in Section 4.1 and the $V_{\text{max}} - M$ relation in Figure 1. Note that the galaxy IC 1613 is only slightly less luminous than NGC 6822 but is approximately 370 kpc closer to M31 and 300 kpc farther from the MW.

* In order to avoid bias, these pairs are indicated with dashed lines in Figures 4, 5, 18, and 19 and have been excluded from Figures 6, 7, 8, 11, 12, and 13 because they have large companions at ~ 1 Mpc distances.

Table 1. Properties of the twelve ELVIS pairs together with associated properties of the MW/M31 pair, where appropriate. Detailed information about the individual halos that make up these pairs is given in Table 2, where they are referred to by the same names used in Column 1.

these two pairs entirely, or show the affected systems with dashed lines.

Figure 2 shows visualizations of our LG analogs colored by the locally smoothed density; each box renders a cube 1.5 Mpc on a side centered on the midpoint of the two hosts. Pair names are indicated and the visualizations are rotated such that the pair is aligned with the horizontal axis, though not necessarily with an orientation that maximizes the apparent separation. Each of these images is fully resolved without contamination from low-resolution particles, so the shape of the density fields represented are accurate. There are a number of features of interest in these images. For example, it is readily apparent that Sonny (of Sonny & Cher in the bottom row) is undergoing a major merger. It has a subhalo of $V_{\text{max}} = 115 \text{ km s}^{-1}$, which is comparable to the host halo's $V_{\text{max}} = 180 \text{ km s}^{-1}$ — not unlike M33 paired with M31. Also, the third massive object near Siegfried & Roy (as discussed above) is evident in the bottom-right panel. As we will discuss below, Zeus & Hera (upper left) furnishes a particularly good match to the Local

Group in many observational comparisons — the 89 km s^{-1} subhalo of Hera is shown on the right.

We list the properties of the individual halos that comprise each pair in Table 2 along with comparative information for the Milky Way and M31, when appropriate. A similar list for the isolated mass-matched analogs is given in Table 3. In each table, Columns 2 through 5 list M_{v} , V_{v} , V_{max} , and R_{v} , respectively. Column 6 gives a measure of the halo concentration, $c_{-2} \equiv R_{\text{v}}/r_{-2}$, where r_{-2} is the radius where ρr^2 peaks (equivalent to the concentration parameter for halos that follow Navarro et al. (1996, NFW) profiles). Column 7 provides a measure of the halo formation redshift, $z_{0.5}$, defined when the main progenitor first obtains half its current mass. Columns 8 and 9 list the number of $V_{\text{max}} > 8 \text{ km s}^{-1}$ subhalos within R_{v} and 300 kpc, respectively, and column 10 lists the V_{max} of the largest subhalo within 300 kpc. Column 11 gives R_{res} , the radius of the largest sphere within which there are no low-resolution particles (an indication of the high-resolution volume size). Columns 12 and 13 list the number of particles (in millions,

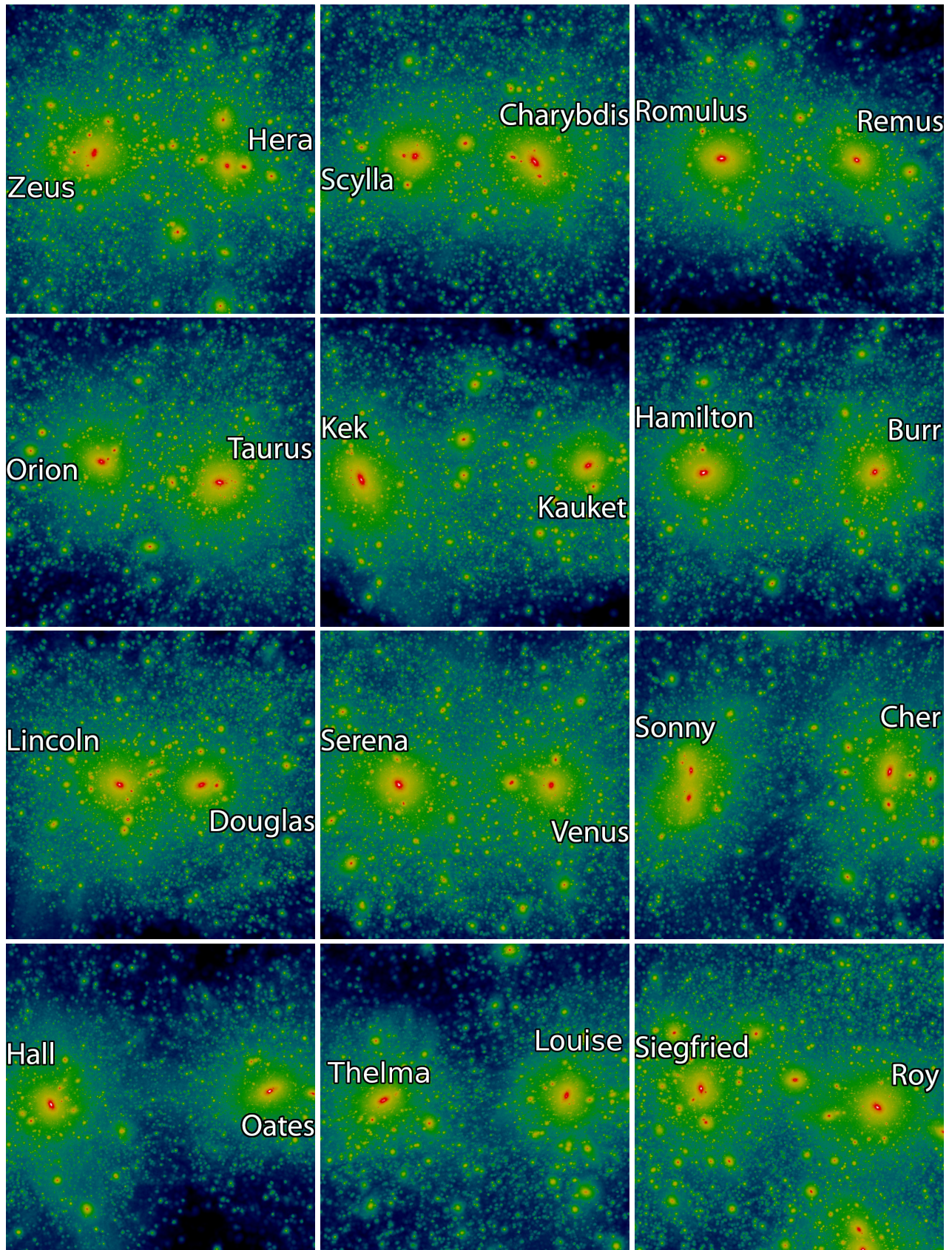


Figure 2. Visualizations of the ELVIS pairs, shown in cubes 1.5 Mpc on a side, each centered on the mean center of the pair with names given.

Halo	M_V ($10^{12}M_\odot$)	V_V (km/s)	V_{\max} (km/s)	R_V (kpc)	c_{-2} ^a	$z_{0.5}$ ^b	N_{halos}^c ($< R_V$)	N_{halos}^d (< 300)	$\text{Max } V_{\max}^e$ (km/s)	R_{res}^f (Mpc)	N_p^g ($< R_{\text{res}}$)	N_{halos}^h ($< R_{\text{res}}$)
Hera	1.30	140	159	285	7.9	0.79	397	435	89	1.33	39M	3,348
Zeus	2.67	178	203	362	5.6	1.08	1,029	880	70	1.92	44M	3,955
Scylla	1.62	151	179	306	6.4	1.24	577	567	84	1.28	36M	3,171
Charybdis	2.35	171	208	346	7.6	0.89	896	785	77	1.91	47M	4,368
Romulus	1.90	159	197	323	9.6	1.57	623	579	54	1.76	30M	2,427
Remus	1.24	138	177	280	12.3	1.53	440	463	40	1.42	26M	2,027
Orion	2.84	182	225	369	5.3	1.61	955	775	47	1.60	35M	2,784
Taurus	1.19	136	169	276	10.9	1.08	383	419	61	1.21	31M	2,321
Kek	2.19	167	205	338	13.7	0.64	685	609	43	1.87	39M	3,333
Kauket	1.06	131	157	266	9.6	1.10	388	426	64	1.56	32M	2,687
Hamilton	1.76	155	197	315	9.9	1.47	582	560	62	1.39	28M	2,494
Burr	1.50	147	173	299	10.6	1.18	613	615	39	1.48	29M	2,529
Lincoln	2.55	176	199	356	8.4	1.36	941	780	75	1.27	31M	2,559
Douglas	1.34	142	169	287	9.6	0.99	412	430	89	1.32	31M	2,558
Serena	2.81	181	222	368	14.4	1.77	911	743	61	1.48	51M	4,418
Venus	1.45	145	156	295	1.8	0.98	612	623	83	1.39	45M	3,879
Sonny	1.89	159	180	322	2.4	0.30	664	637	115	0.97	20M	1,480
Cher	1.80	156	171	317	11.0	0.66	580	552	81	1.12	27M	2,082
Hall	1.52	148	180	299	10.3	1.04	437	438	50	1.35	23M	1,560
Oates	1.20	136	167	277	8.4	0.62	317	346	76	1.01	17M	1,085
Thelma	1.34	141	169	287	7.1	1.44	421	438	48	0.91	18M	1,379
Louise	1.03	130	157	263	17.0	1.61	357	407	54	0.80	11M	928
Siegfried	2.17	166	195	337	6.5	0.67	827	734	62	1.09	46M	3,674
Roy	2.14	166	194	336	11.1	1.14	702	628	64	1.15	53M	4,325
Milky Way	$1.6^{+0.8}_{-0.6}$ ⁱ	150^{+22}_{-22}	–	304^{+45}_{-45}	–	–	–	$\geq 27^j$	88^k	–	–	–
M31	1.8 ± 0.65^l	156^{+17}_{-22}	–	317^{+35}_{-44}	–	–	–	$\geq 32^j$	130^m	–	–	–

^a Halo concentration defined as $c_{-2} \equiv R_V/r_{-2}$, where r_{-2} is the radius where ρr^2 peaks. This parameter is equivalent to the NFW concentration for halos that follow perfect NFW profiles (Navarro et al. 1996).

^b Formation time proxy defined as the redshift z when the main progenitor mass first equaled $0.5 M_V(z=0)$.

^c Number of subhalos within R_V with $V_{\max} > 8$ km/s.

^d Number of subhalos within 300 kpc with $V_{\max} > 8$ km/s.

^e V_{\max} value of the largest identified subhalo within 300 kpc.

^f The high-resolution radius, defining a sphere centered on the halo within which there is zero contamination from low-resolution particles.

^g Number of particles in millions (rounded to the nearest million) within the high-resolution radius R_{res} .

^h Number of subhalos within R_{res} with $V_{\max} > 8$ km/s.

ⁱ Taken from Boylan-Kolchin et al. (2013) with 90% c.l. quoted.

^j As enumerated in McConnachie (2012).

^k The LMC, from Olsen et al. (2011)

^l Combining results from Fardal et al. (2013) and van der Marel et al. (2012) who obtain $M_V^{M31} = (2.1 \pm 1.0) \times 10^{12}$ and $(1.5 \pm 0.8) \times 10^{12}$, respectively, with 2- σ errors quoted.

^m The Triangulum galaxy (M33), from Corbelli (2003)

Table 2. Properties of the twenty-four halos that comprise our Local Group sample, along with the properties of the MW and M31, where appropriate. The halos are listed in the same order as in Table 1, and identified by the names in Column 1 of that Table. All values in this table are relative to the center of the each host; equivalent properties for the isolated sample are listed in Table 3, where identical names with preceding i 's may be used to identified mass-matched analogues. The table is discussed in § 2.

rounded to the nearest million) and number of identified halos (with $V_{\max} > 8$ km s⁻¹) within R_{res} for each halo.

Note that in what follows we will occasionally present results for a region we define as the Local Volume – the union of two spheres of radius 1.2 Mpc centered on each host. As can be seen from Column 11 of Table 2, four of our pairs are technically contaminated in this region (Sonny & Cher, Hall & Oats, Thelma & Louise, and Siegfried & Roy). However

the mass fraction of low-resolution particles in the effected volumes is minimal (0.01%, 0.007%, 0.06%, and 0.0008% respectively) so the practical effects on our results should be negligible (see, e.g. Oñorbe et al. 2013).

Before devoting the next section to a detailed comparison of paired vs. unpaired hosts, we mention that we find no statistical difference in the c_{-2} and $z_{0.5}$ distributions between the two sets. Though two of our halos (Serena and

Halo	M_v ($10^{12}M_\odot$)	V_v (km/s)	V_{\max} (km/s)	R_v (kpc)	c_{-2} ^a	$z_{0.5}$ ^b	N_{halos}^c ($< R_v$)	N_{halos}^d (< 300)	$\text{Max } V_{\max}^e$ (km/s)	R_{res}^f (Mpc)	N_p^g ($< R_{\text{res}}$)	N_{halos}^h ($< R_{\text{res}}$)
iHera	1.22	137	163	278	7.9	0.8	420	450	41	1.54	17M	1,348
iZeus	2.59	176	205	358	5.5	1.3	925	773	60	1.76	27M	2,312
iScylla	1.59	150	176	304	9.9	0.97	437	436	84	1.56	20M	1,500
iCharybdis	2.29	169	207	343	13.7	1.4	758	643	51	1.72	25M	2,125
iRomulus	1.97	161	186	327	11.3	0.88	792	734	75	1.89	21M	1,899
iRemus	1.31	141	166	285	8.0	0.91	494	515	54	1.40	14M	1,261
iOrion	2.84	182	218	369	4.9	1.64	1,179	1,015	54	2.06	37M	3,315
iTaurus	1.23	138	165	279	10.4	1.36	453	481	46	1.75	14M	1,315
iKek	2.41	172	204	349	5.5	0.74	705	618	71	1.63	27M	2,267
iKauket [†]	1.02	129	157	262	11.1	0.97	278	327	39	2.12	21M	1,730
iHamilton	1.86	158	203	321	14.2	2.11	566	523	57	1.55	17M	1,309
iBurr	1.56	149	179	302	13.6	0.75	548	540	66	1.61	15M	1,279
iLincoln	2.62	177	213	359	13.8	0.89	813	702	83	1.35	27M	2,017
iDouglas	1.30	140	180	285	16.1	1.76	375	383	49	1.93	15M	1,107
iSerena	2.67	178	212	361	11.4	1.15	952	817	81	1.66	26M	2,218
iVenus	1.39	143	179	291	14.3	1.41	461	483	46	2.15	32M	2,684
iSonny	1.68	153	187	310	4.5	0.69	647	632	117	2.01	20M	1,877
iCher	1.92	160	170	324	6.4	0.6	701	660	63	2.23	22M	1,888
iHall [◊]	1.71	148	172	300	6.0	1.13	528	528	92	1.59	16M	1,264
iOates	1.20	136	157	277	8.4	0.72	444	478	78	1.58	13M	1,068
iThelma	1.39	143	188	291	9.6	1.56	407	421	37	1.95	14M	1,043
iLouise	1.01	129	155	261	8.4	1.22	378	414	49	2.41	14M	1,253
iSiegfried	2.40	172	211	349	11.1	1.42	733	643	55	1.36	21M	1,589
iRoy	2.26	169	205	342	3.9	1.11	844	769	103	1.75	22M	1,850
iScilla HiRes	1.61	150	175	305	9.5	0.95	419 (3,824)*	413 (3,770)*	87	1.54	155M	1,491 (12,509)*
iKauket HiRes [‡]	1.03	130	158	263	11.8	1.0	277 (2,279)*	324 (2,620)*	38	0.4	56M	446 (3,493)*
iHall HiRes	1.67	152	167	309	5.8	1.07	608 (5,266)*	592 (5,114)*	93	1.59	125M	1,286 (11,176)*

^a Halo concentration defined as $c_{-2} \equiv R_v/r_{-2}$, where r_{-2} is the radius where ρr^2 peaks. This parameter is equivalent to the NFW concentration for halos that follow perfect NFW profiles (Navarro et al. 1996).

^b Formation time proxy defined as the redshift z when the main progenitor mass first equaled $0.5 M_v(z=0)$.

^c Number of subhalos within R_v with $V_{\max} > 8$ km/s.

^d Number of subhalos within 300 kpc with $V_{\max} > 8$ km/s.

^e V_{\max} value of the largest identified subhalo within 300 kpc.

^f The high-resolution radius, defining a sphere centered on the halo within which there is zero contamination from low-resolution particles.

^g Number of particles in millions (rounded to the nearest million) within the high-resolution radius R_{res} .

^h Number of subhalos within R_{res} with $V_{\max} > 8$ km/s.

[†] iKauket was initialized at $z = 250$ for both the fiducial and HiRes runs.

[◊] Differences in the phase of subhalo orbits between this run and the HiRes equivalent result in the largest subhalo ($V_{\max} = 93 \text{ km s}^{-1}$) being located just beyond R_v at the fiducial resolution. To show convergence with the HiRes run, we include the mass of that halo in the virial mass of iHall and list it in Column 10, though it is just beyond 300 kpc. The uncorrected substructure counts are also divergent, but the number of objects within 400 kpc agrees within 5%. The uncorrected mass ($1.53 \times 10^{12} M_\odot$) also agrees with the paired halo, Hall, to within 1%.

* Values in parentheses correspond to subhalo counts down to $V_{\max} > 4$ km/s, the estimated completeness limit of the HiRes simulations.

[‡] This halo was initialized with a smaller Lagrange volume of high-resolution particles than the rest, which is why it has an anomalously small high-resolution radius.

Table 3. Properties of the twenty-four isolated halos that are mass matched to the halos in our Local Group analogues. The name identifies the paired halo with a nearly identical mass, the properties of which are listed in Table 2, and the preceding *i* indicates an isolated analogue. Columns are identical to those in Table 2. The last three rows correspond to the HiRes simulations of three halos.

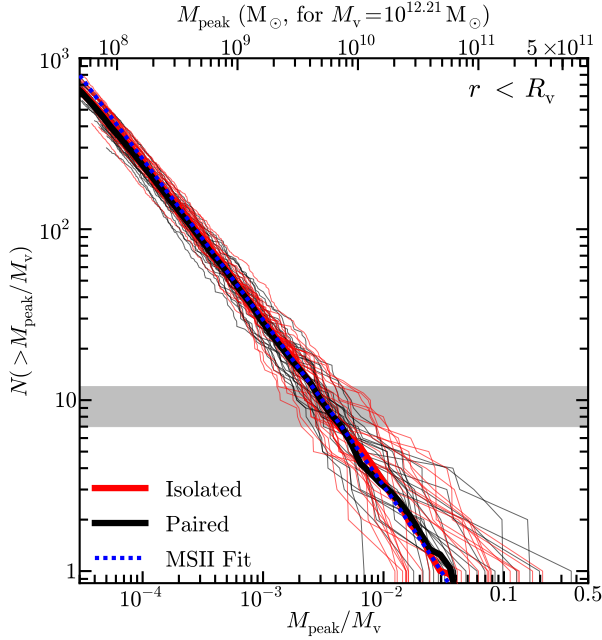


Figure 3. Cumulative subhalo peak mass function (M_{peak}) normalized by host M_v for each isolated (thin red lines) and paired (thin black lines) host. All objects within R_v are plotted. The average for each population is shown by the thick lines of corresponding color. Statistically, the mass functions for paired and isolated hosts are indistinguishable, though the halo-to-halo scatter is large. The upper axis is scaled to the subhalo M_{peak} values assuming a host virial mass of $M_v = 1.6 \times 10^{12} M_\odot$, which is our fiducial MW mass. Thin lines are truncated at $M_{\text{peak}} = 6 \times 10^7 M_\odot$, the completeness limit of our simulation catalogs. The grey band shows the range in number of satellites around the Milky Way and M31 with stellar masses above $10^6 M_\odot$; from this band, one can see that such galaxies would be expected to form in halos more massive than $M_{\text{peak}} \simeq 3 \times 10^{-3} M_v \simeq 5 \times 10^9 M_\odot$.

Sonny) that happen to be members of pairs have anomalously low c_{-2} values, we suspect that in Sonny’s case this is a result of an ongoing major merger. The median formation redshifts for our paired and unpaired samples are both $z_{0.5} \simeq 1.1$, with no indication that paired halo formation times correlate.

The lack of difference in the $z_{0.5}$ distribution between the two samples is consistent with the comparison made by Forero-Romero et al. (2011) using similarly paired halos found in the Bolshoi simulations. These authors point out that the three LG-like pairs identified in the constrained CLUES simulations have anomalously early formation times, all three with half-mass formation times $z_{0.5} \gtrsim 1.5$. Three of our twelve paired systems are similarly early-forming (Romulus & Remus, each with $z_{0.5} \simeq 1.6$), Orion & Taurus (with $z_{0.5} = 1.6$ and 1.3 , respectively), and Thelma & Louise (with $z_{0.5} = 1.4$ and 1.6).

3 PAIRED vs. ISOLATED GALAXIES

3.1 Halo abundances

We begin by examining the abundance of dark matter structures, characterized by their M_{peak} values, within various ra-

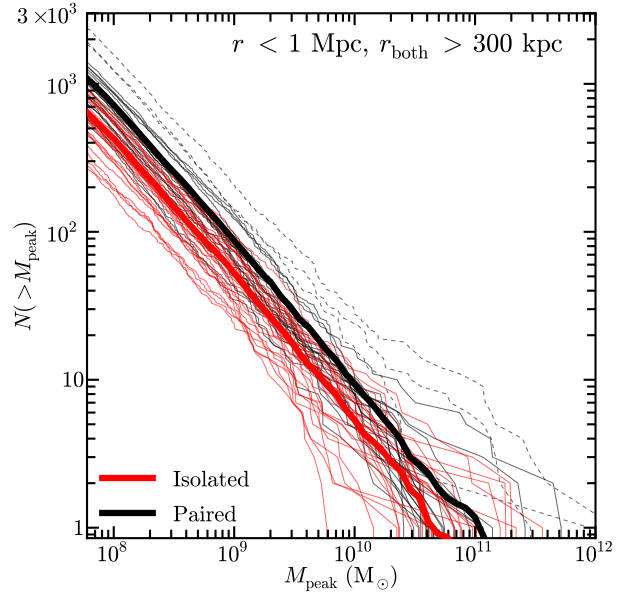


Figure 4. Cumulative counts, as a function of M_{peak} , for halos that are between 300 kpc and 1 Mpc of any host. The paired population (black) has an amplitude that is approximately 80% larger at fixed M_{peak} than that of the isolated analogs (red). The environment around a LG pair thus differs noticeably from that of an isolated MW-size halo, even though such differences are not manifest within the virial radius (Figure 3).

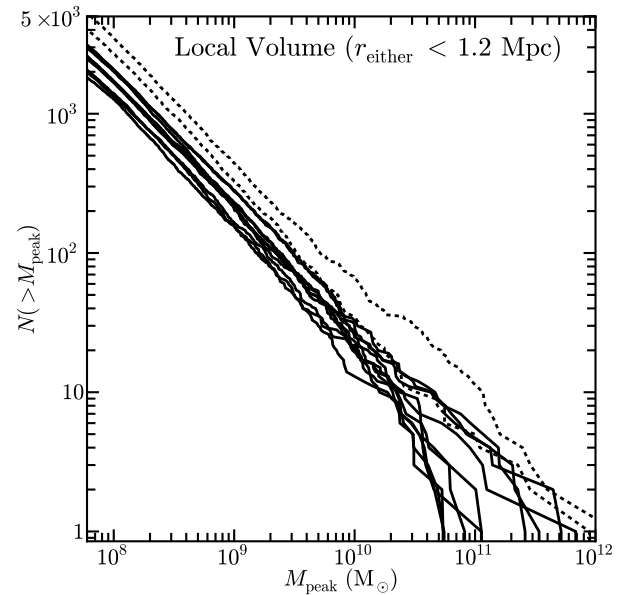


Figure 5. The M_{peak} functions around the LG pairs; each line represents a pair of giants and includes all halos (excluding the MW and M31 analogs) within 1.2 Mpc of either host, which we define as the Local Volume. Two pairs contain a third large system within the volume and are thus shown as dashed lines. We predict ~ 2000 – 3000 objects with $M_{\text{peak}} > 6 \times 10^7 M_\odot$ within the region.

dial boundaries; counts as a function of V_{\max} are presented in Appendix B.

Figure 3 shows the cumulative M_{peak} functions for subhalos within R_v , normalized to the host halo virial mass M_v , for each of the forty-eight hosts in ELVIS. Isolated hosts are shown as thin red lines and the paired hosts are plotted in black. The two distributions clearly overlap. The thick lines denote the mean cumulative count at fixed M_{peak}/M_v for the isolated (red) and paired (black) populations. Both distributions are well fit at the low mass end by a power-law:

$$N_v(> M_{\text{peak}}) = 3.85 \left(\frac{M_{\text{peak}}}{0.01 M_v} \right)^{-0.9}. \quad (1)$$

Within R_v , subhalo counts within isolated and paired halos in ELVIS are indistinguishable. Even for high-mass subhalos, where the intrinsic scatter in the counts is large, the means agree well. The blue dashed line, which sits practically on top of the ELVIS means, shows the mean power-law fit obtained by Boylan-Kolchin et al. (2010) for subhalos in a large sample of Milky Way-mass halos from the Millennium-II Simulation (Boylan-Kolchin et al. 2009). The same fit also matches the substructure counts from the Aquarius simulations (Springel et al. 2008) well. The agreement between our simulations and MS-II/Aquarius is remarkable, especially given that the cosmology of these older simulations is slightly different from our adopted values, which are based on more recent constraints.

Broadly speaking, the scatter in subhalo counts among halos also agrees between the two samples. At small masses ($M_{\text{peak}}/M_v \lesssim 10^{-3}$) we find that the standard deviation divided by the mean approaches $\sigma/\langle N \rangle \simeq 0.15$, and that the scatter increases towards higher masses, with $\sigma/\langle N \rangle \simeq 0.4$ at $M_{\text{peak}} \simeq 0.01 M_v$. This result is consistent with an intrinsic halo-to-halo scatter of $\sim 15\%$ in the abundance of substructure reported elsewhere (Boylan-Kolchin et al. 2010; Busha et al. 2011; Wu et al. 2013).

Though we do not plot it, the $z = 0$ (bound) mass functions also agree well within R_v and are both well fit by

$$N_v(> M) = 1.11 \left(\frac{M}{0.01 M_v} \right)^{-0.95}, \quad (2)$$

though the scatter is slightly larger than in the M_{peak} function ($\sigma/\langle N \rangle \sim 0.2$ at small masses).

One take-away from this initial result is that predictions for subhalo counts within the virial radius from previous high resolution simulations that studied isolated MW-size hosts (e.g. Diemand et al. 2008; Kuhlen et al. 2008; Springel et al. 2008) are not expected to be significantly different than those for paired halos like the Milky Way and M31.

At distances beyond the virial radii of either host, the presence of a massive companion should affect halo abundances. To compare the counts at large distances between isolated and paired Milky Way-size halos, we must avoid the bias that would be introduced by simply counting all halos at a given distance, as many will be subhalos of the M31 analog in the paired systems. We attempt to remove this bias by defining a region around each host that we call the ‘‘Local Field’’: a spherical shell between 300 kpc and 1 Mpc of the center of that host, but excluding the region within 300 kpc of the center of the other giant. That is, no subhalos of either LG giant analog are included in this region.

We plot the M_{peak} function for these Local Field regions

around all the ELVIS halos in Figure 4. The environment surrounding a typical LG-like halo is richer than that around an isolated system, even when the partner’s subhalos are removed. Specifically, the average relations are again well fit at the low mass end by power laws, but the normalization for the paired sample is about 80% higher than that of the isolated sample:

$$N_{0.3-1}(> M_{\text{peak}}) = N_0 \left(\frac{M_{\text{peak}}}{10^{10} M_\odot} \right)^{-0.9}, \quad (3)$$

with $N_0 = 6.4$ for the isolated sample and $N_0 = 11$ for the paired sample. The dashed lines in Figure 4 indicate the two halos that have a large companion within the 0.3 – 1 Mpc region (see § 2.3 and Table 1). It is possible that these systems are poor comparison sets to the Local Group, which appears to lack such a galaxy (Table 1). If we remove the dashed lines from the fit, the normalization for the paired systems becomes $N_0 = 9.2$, which is $\sim 56\%$ higher than that for the isolated sample (removing the isolated counterparts to those halos also gives a slightly lower normalization $N_0 = 5.9$). While the distributions show some overlap, the presence of a paired companion appears to bias the overall large-scale environment to be substantially richer in small halos, even when the subhalos of the paired host are excluded from the counts.

Figure 5 presents total halo number counts as a function of M_{peak} within a bi-spherical volume defined by overlapping spheres of radius 1.2 Mpc of each paired host. There is one line for every EVLIS pair, thus each can be regarded as a realization of the Local Group itself. The dashed lines indicate the two pairs that have large companions in the region, possibly making them less than ideal comparison sets for the Local Group. Neglecting those two systems, the group-to-group scatter in this Local Volume mass function is remarkably tight, spanning less than a factor of ~ 2 over all ten realizations for masses $M_{\text{peak}} \lesssim 10^{10} M_\odot$. In total, the best LG analogs in the ELVIS suite have 2000 – 3000 halos with $M_{\text{peak}} > 6 \times 10^7 M_\odot$ in this Local Volume region. Of course, many of these small halos likely contain galaxies that are either devoid of stars entirely, or too faint to detect with current methods. We investigate implications for the number of observable galaxies throughout this region in §4.

3.2 Halo Dynamics

We expect that the presence of M31 alters the dynamical structure of the Milky Way’s local environment relative to the environment of an isolated analog. While we find that, within ~ 300 kpc of the hosts, the paired and isolated samples have indistinguishable subhalo kinematics, regions beyond this distance show distinct kinematical differences.

Figure 6 shows stacked distributions of radial and tangential velocities for $M_{\text{peak}} > 6 \times 10^7 M_\odot$ halos having distances between 800 kpc and 1.2 Mpc of a giant. Note that in these histograms, we compute the distance to both of the hosts and only use the smaller of the two distances (i.e., all halos at distance r from one host are at least that same distance r from the other host). Regions surrounding isolated hosts are shown in red while regions around paired systems are in black. The kinematic distinction is clear: paired halos are both kinematically hotter and show an excess of systems that are outflowing at this radius. As we discuss in the next

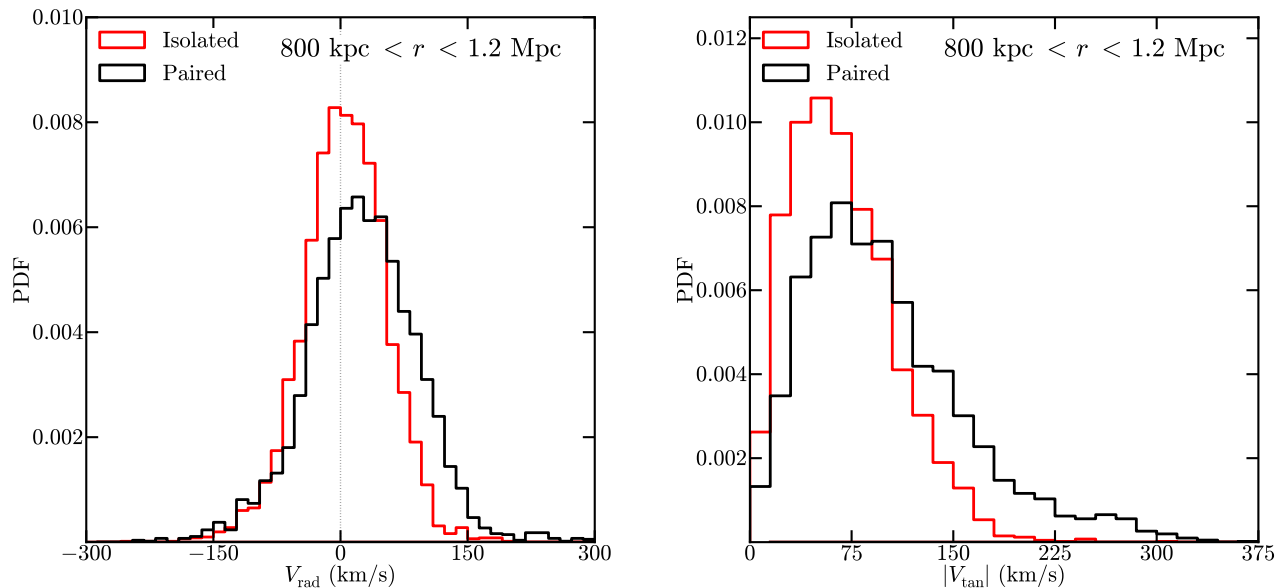


Figure 6. Stacked distributions of radial (left panel) and tangential (right panel) velocities for halos around the isolated (red) and paired (black) halos at distance of $0.8 - 1.2$ Mpc from the *nearest* host. While the distributions for paired and isolated halos are the same within R_v (not plotted), the differences become pronounced at large radii, with paired environments being substantially hotter. While essentially all halos ~ 1 Mpc from isolated MW analogs have $V_{\text{tan}} < 200 \text{ km s}^{-1}$, a large fraction around LG analogs have $V_{\text{tan}} > 200 \text{ km s}^{-1}$. It is also apparent that while the radial velocities of halos at ~ 1 Mpc distance from isolated MW-like hosts are centered on zero, the paired analogs have an excess population of outflowing systems. These outflowing systems include a “backslash” population that is larger among pairs (see § 3.3) and also objects that have yet to turn around from the Hubble flow (the zero velocity surface is centered on the pair at ~ 1 Mpc distance, not the individual host). One broad implication of this Figure is that in order to correctly predict the large-scale velocity field around the MW, one must account for the presence of M31.

subsection, this enhanced population of outflowing halos includes a large number of objects that were once within the virial radius of one of the giants. This fraction appears to be higher in paired hosts. A complication when interpreting the radial velocity figure is that the zero-velocity/turn-around surface (at ~ 1 Mpc distance) for the pairs is centered between the hosts rather than on the main halo as it is for the isolated analogs. This means that some fraction of the halos in this diagram may not have turned around from the Hubble flow.

In the histograms shown in Figure 6, we have removed halos belonging to the pairs Siegfried & Roy and Serena & Venus. As discussed above, these pairs have a particularly large halo within 1.2 Mpc of one of the hosts, and therefore may be poor analogs to the real Local Group. Including them only serves to make the overall paired histograms even hotter compared to the isolated analogs.

3.3 Backslash Halos

Here we investigate the dynamical histories of each small halo in the vicinity of our MW analogs at $z = 0$, and specifically ask whether a halo has been within the virial radius of either giant since $z = 5$. If so, then in principle, environmental effects such as ram pressure, harassment, or strangulation could have quenched the galaxy it hosts (Kawata & Mulchaey 2008; Boselli et al. 2008; Grcevich & Putman 2009; Woo et al. 2013; Phillips et al. 2013). We refer to

previously-interacted objects of this kind as “backslash” halos (e.g., Gill et al. 2005 and references therein).

Figure 7 presents the differential fraction of halos that are backslash objects as a function of distance from each host in radial bins of width $R_v/2$. Systems around our LG-analogs are shown in black, where the distance assigned is the minimum of the distances to the two giants in the group. As in Figure 6, we have removed halos belonging to the two pairs in our sample with large companions at ~ 1 Mpc distance. The subsample of halos that meet the radial cut from the center of both giants simultaneously are shown in cyan. The isolated sample is shown in red. We indicate with open symbols bins where the full halo sample was not used, either due to contamination at large radii or because there are no halos that meet the radial cut in the bin. The points correspond to the average over all hosts and the error bars denote the full width of the distribution, measured system-by-system.

Unsurprisingly, the backslash fraction is largest at small radii. In the regions spanning $1 - 1.5 R_v$, typically 70% of halos have been within R_v since $z = 5$, though that number can be as high as 80% in some cases (also see Mamon et al. 2004; Gill et al. 2005). The interaction fraction in the environment of LG-like pairs is systematically higher than in isolated analogs at large radii, and the overlapping volume (cyan) is particularly rich in objects that have interacted. Indeed, the shared region in the real LG may be the best hunting ground for potential backslash candidate dwarfs.

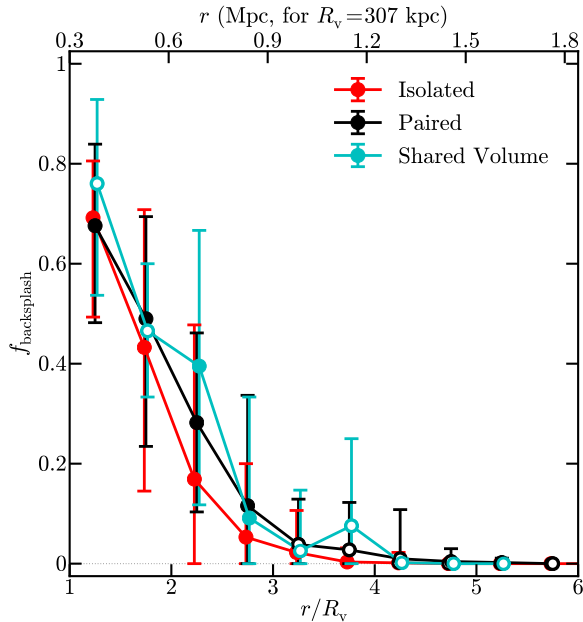


Figure 7. The fraction of $M_{\text{peak}} > 6 \times 10^7 M_{\odot}$ halos at $z = 0$ that have been within R_v of a MW size host as a function of r/R_v from the center of each host. The points show the average in each radial bin and the error bars denote the full width of the distribution over all hosts. The red line corresponds to the isolated sample, and the black line corresponds to paired hosts, where the distance is to the nearest of the two giants. The cyan line also counts systems in the paired simulations, but counts only those systems that simultaneously meet the radial cut for both hosts. The most likely location for backsplash halos is in this shared volume and between $1 - 2 R_v$ of both hosts (i.e., in between the two halos rather than on one side or the other of the LG pair).

Remarkably, in our LG-analog systems, the probability that a halo has interacted only drops to zero at approximately $5 R_v$ (~ 1.5 Mpc). Expressed cumulatively (rather than differentially), we find that the overall fraction of backsplash halos within the 1.2 Mpc Local Volume regions of our paired hosts ranges from 30% to 52%.

How might backsplash halos be distinguished observationally throughout the Local Group? In Figure 8, we compare the relative tangential and radial velocities of backsplash halos in the $r = 400 - 800$ kpc radial bins to those that have never accreted. Here we limit ourselves to paired hosts. As in Teyssier et al. (2012), we find that backsplash halos tend to be outflowing from the host that they have interacted with, whereas those that have not yet accreted are preferentially inflowing. As the right plot shows, we also expect backsplash halos to have low tangential velocities compared to those that have never been within R_v . The implication is that backsplash systems are more likely to be on radial orbits and to be on their way out. At the same time, there is significant overlap in the distributions and it is difficult to disentangle the populations on these specific kinematic properties alone. We reserve a more thorough analysis of this question for a future paper.

4 EXPECTATIONS FOR THE LOCAL GROUP

As the previous section showed, number counts and velocity distributions within R_v are consistent between isolated and paired MW-size halos, but differences are evident at greater radii. In this section, we will focus on predictions in the ~ 1 Mpc scale environment around the Milky Way and will present results for the paired sample only.

4.1 Stellar Mass Functions

Although the ELVIS simulations are dissipationless, the abundance matching (AM) technique (Kravtsov et al. 2004; Vale & Ostriker 2004; Conroy et al. 2006; Behroozi et al. 2013c; Moster et al. 2013) makes it possible to assign stellar masses to dark matter halos and convert the halo mass functions in Figures 3 and 5 into reasonably proxies for stellar mass functions. The connection between galaxy mass and halo mass remains highly uncertain at low masses $M_{\star} \lesssim 10^8 M_{\odot}$, however, as it is difficult to measure luminosity functions over large volumes for dim galaxies. In this sense, comparisons to galaxy counts within the Local Group, where luminosity functions are more complete, can help test and refine AM relationships that have been built upon cosmological samples.

Figure 9 shows the $z = 0$ abundance matching relation published by Behroozi et al. (2013c) as the orange line. The plotted relation becomes dashed at $M_{\star} < 10^{8.5} M_{\odot}$, reflecting the approximate completeness limit of the SDSS-derived stellar mass function of Baldry et al. (2008), on which the Behroozi et al. (2013c) relation was based. The black line shows a modified version of the Behroozi et al. (2013c) relation, motivated by the updated stellar mass function of Baldry et al. (2012), who found flatter faint-end slope ($a_{\star} = -1.47$ vs -1.6 in Baldry et al. 2008) using the Galaxy And Mass Assembly (GAMA) survey (Driver et al. 2011), which probes ~ 2 magnitudes deeper than SDSS, albeit over a smaller area of sky. In this modified relation we have simply altered the asymptotic slope α to be 1.92 in equation 3 of Behroozi et al. (2013c), such that at small masses $M_{\star} \propto M_{\text{peak}}^{1.92}$. This is based on the expectation that $\alpha = (1 + a_{\text{dm}})/(1 + a_{\star})$ and assuming an asymptotic halo mass function slope of $a_{\text{dm}} = -1.9$ (e.g. Jenkins et al. 2001). As we show below, this modified relation does a better job in reproducing dwarf galaxy counts in the Local Group than the original Behroozi et al. (2013c) formulation. Our preferred relation is well-described by a power law for $M_{\star} < 10^8 M_{\odot}$:

$$M_{\star}(M_{\text{peak}}) = 3 \times 10^6 M_{\odot} \left(\frac{M_{\text{peak}}}{10^{10} M_{\odot}} \right)^{1.92}. \quad (4)$$

In the mass range of interest, this modified $M_{\star} - M_{\text{peak}}$ relation is more similar to the abundance matching prescription presented in Moster et al. (2013).

Figure 10 shows the stellar mass functions of galaxies within 300 kpc of either the Milky Way (dark blue) or M31 (cyan) compared to the predicted stellar mass functions for our ELVIS pairs based on the two AM relations shown in Figure 9. For the galaxy stellar mass functions, we use the masses from Woo et al. (2008), where available, and the luminosity data cataloged in McConnachie (2012), assuming $M_{\star}/L = 2$, otherwise. The lines become dashed where in-

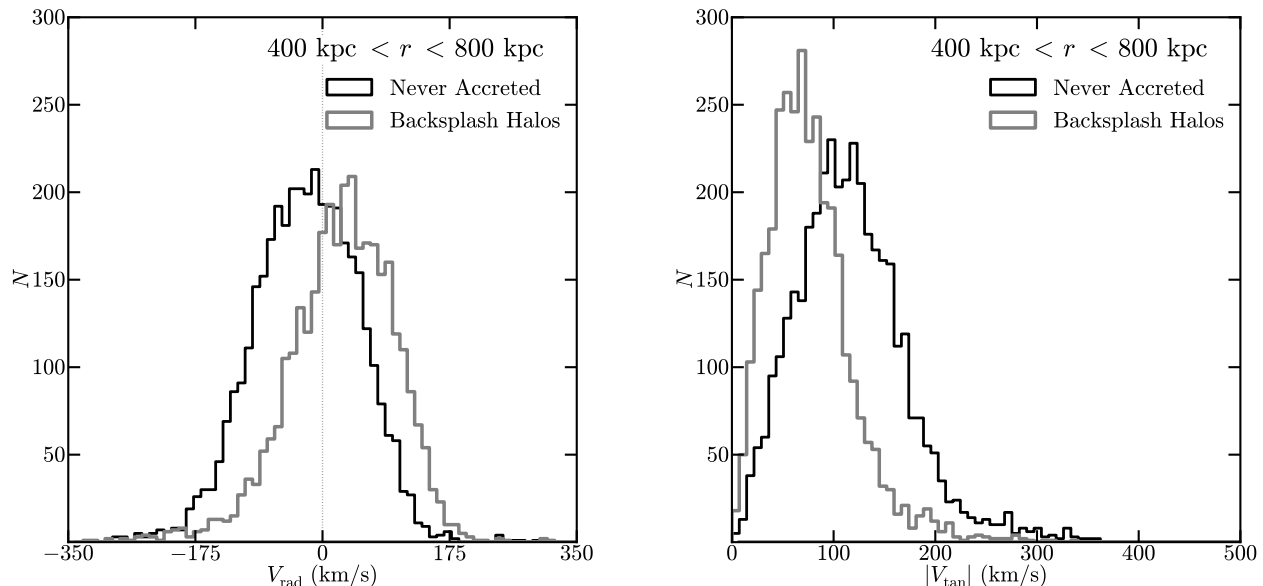


Figure 8. The radial (left) and tangential (right) velocity distributions of field halos in the spherical shell 400–800 kpc from the center of each paired host, truncated in the same manner as Figures 6 and 7. The black lines plot only those halos that have never been within R_v and the grey lines includes only backsplash halos. The latter are comparatively outflowing with relatively low tangential velocities. Note that in this figure we have excluded the two pairs in our sample with large companions at ~ 1 Mpc distance.

completeness may become an issue (see, e.g. Koposov et al. 2008; Tollerud et al. 2008; Richardson et al. 2011; Yniguez et al. 2013).

The orange lines in Figure 10 show the stellar mass functions for each of the 24 paired ELVIS hosts derived from the $M_*(M_{\text{peak}})$ relation of Behroozi et al. (2013c). The median relation is shown by the thick line. For this exercise we have applied the $z = 0$ relation to all subhalos using their M_{peak} masses, which follows the prescription of Behroozi et al. (2013c). As can be seen, the standard Behroozi et al. (2013c) relation gives a stellar mass function that is too steep, over-predicting the count of galaxies smaller than $M_* \simeq 10^7 M_\odot$ significantly. Our modified relation (applied to ELVIS halos in black) does a better job by assigning less stellar mass to smaller halos. For this reason we will adopt this preferred AM relation in all relevant figures to follow. In magenta, we highlight the satellites of the host Hera, which happens to be a particularly good match to the data (at least in the regime where it is likely complete) in this and several figures that follow. Based on our preferred AM relation, we predict $\sim 200 - 300$ galaxies with $M_* \geq 10^3 M_\odot$ within 300 kpc of the MW / M31.

We note that both AM prescriptions under-predict the satellite stellar mass function for the MW / M31 at $M_* \geq 10^8 M_\odot$ when considering the average satellite mass function. At these relatively high masses, however, the halo-to-halo scatter is large and the well-established rarity of LMC-like objects (Boylan-Kolchin et al. 2010; Busha et al. 2011; Tollerud et al. 2011) biases the mean result relative to observations of the Local Group. The stellar mass functions around individual hosts with large subhalos, e.g. Hera in magenta, match observations well over four decades in stellar mass after applying the preferred AM relation.

Figure 11 presents stellar mass functions for simulated Local Volumes (unions of 1.2 Mpc spheres around either host) using our preferred AM relation. There is one line for each pair of halos in the ELVIS sample, excluding the two cases that contain a third large halo nearby (detailed in § 2.3). Our AM-based prediction agrees reasonably well with the data for $M_* \gtrsim 5 \times 10^6 M_\odot$, but rises much more steeply towards lower masses, in the regime where the current census is almost certainly incomplete. We highlight the pair Zeus & Hera in magenta. This pair has an M_* function that happens to be very similar to that of the LG. We see that if the AM relation is extrapolated down to $M_* \sim 10^3 M_\odot$ we expect ~ 1000 galaxies within the Local Volume (compared to the ~ 70 systems currently known). Future surveys like those performed with LSST (Ivezic et al. 2008) will help test such extrapolations, exploring the relationship between halo mass and galaxy mass at the very threshold luminosities of galaxy formation.

4.2 HI Mass Functions

While future resolved-star surveys promise to discover faint optical galaxies throughout the Local Volume, HI surveys offer a complementary approach for the discovery of dwarfs in the near-field (Blitz et al. 1999; Blitz & Robishaw 2000; Sternberg et al. 2002; Adams et al. 2013; Faerman et al. 2013). While the faintest dwarfs within ~ 300 kpc of either the MW or M31 are gas-poor dSphs, gas-rich dwarfs are the norm beyond the virial regions of either giant (Grcevich & Putman 2009; McConnachie 2012). Leo T, at distance of ~ 400 kpc from the MW, is an example of a very faint system that is gas-rich ($M_* \simeq M_{\text{HI}} \simeq 10^5 M_\odot$; Ryan-Weber et al. 2008) and apparently falling in to the MW virial radius for

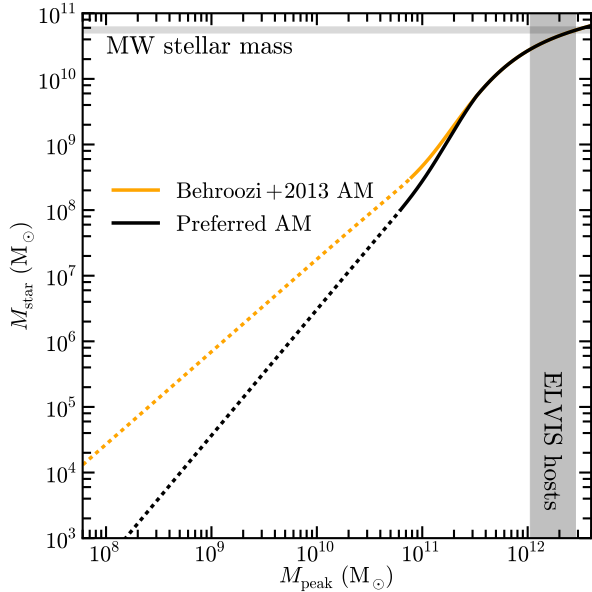


Figure 9. The abundance matching relation between stellar mass and halo mass from Behroozi et al. (2013c, orange line), extrapolated to low halo masses, compared to a modified relation (black) motivated by the updated stellar mass function of Baldry et al. (2012). As shown in Figure 10, this modified relation does a better job of reproducing faint ($M_* \sim 10^6 - 10^8 M_\odot$) galaxies in the Local Group. The two lines are solid over the range where the input stellar mass functions are complete and become dashed in the regime associated with pure extrapolation. For reference, the horizontal grey band shows the stellar mass of the Milky Way from Bovy & Rix (2013). The virial masses of our ELVIS hosts span the vertical grey band. Note that while our halo virial masses are consistent with dynamic estimates of MW and M31 virial masses, they are at the low-mass end of abundance matching expectations for a system with the stellar mass of the Milky Way.

the first time (Rocha et al. 2012). Similar, though possibly even less luminous, objects may fill the Local Volume, and if so, could be detected in blind searches for neutral hydrogen. Recently, for example, the gas-rich galaxy Leo P ($M_{\text{HI}} \simeq 3 M_* \simeq 10^6 M_\odot$) was discovered at a distance of $\sim 1.5 - 2$ Mpc using HI observations (Giovanelli et al. 2013; Rhode et al. 2013).

Here we use the ELVIS suite to provide some general expectations for the HI mass function in the Local Volume. Building off of the results presented in § 4.1, we use our preferred AM relation coupled with an empirically-derived $M_* - M_{\text{HI}}$ relation to assign HI masses to halos in our simulated Local Volumes. Specifically, we fit a power-law relation to the gas-rich dwarfs in the Local Group from McConnachie (2012), ensuring that the gas-fraction relation matches that found by Huang et al. (2012b) at higher masses:

$$M_{\text{HI}} = 7.7 \times 10^4 M_\odot \left(\frac{M_*}{10^5 M_\odot} \right)^{1.2}. \quad (5)$$

Of course, this simple assumption of a one-to-one relation between stellar mass and HI mass is highly idealized. In reality, the gas-to-stellar-mass relation shows a considerable amount of scatter (Kannappan 2004; McGaugh 2005; Stew-

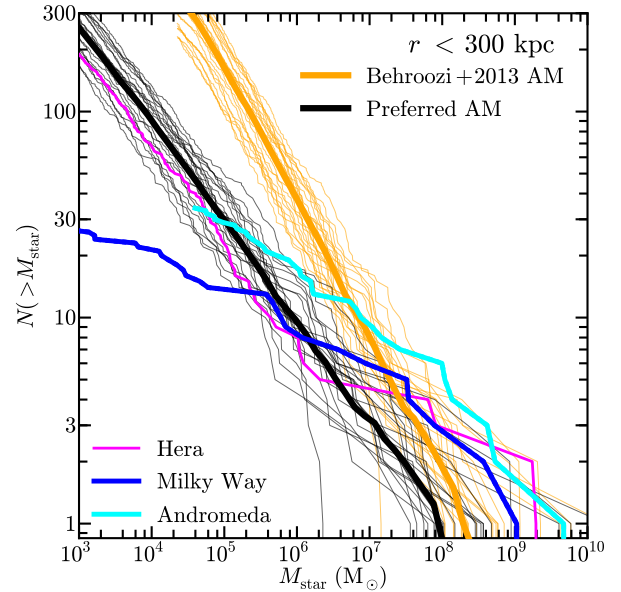


Figure 10. A comparison of observed stellar mass functions within 300 kpc of the MW (blue) and M31 (cyan) with predictions from the ELVIS subhalo catalogs and extrapolated Abundance Matching (AM) relations. The orange lines use the AM prescription of Behroozi et al. (2013c), which adopts a faint-end slope of the luminosity function of -1.6 (Baldry et al. 2008), while the black curves modify the Behroozi relation by assuming a slightly shallower faint-end slope of the luminosity function of -1.47 (Baldry et al. 2012). The standard Behroozi et al. (2013c) relation over-predicts the LG data significantly at $M_* = 5 \times 10^5 M_\odot$, a regime where the census of satellites is believed to be complete. The modified Behroozi relation (given in the text) is a better match to the observed counts.

art et al. 2009; Huang et al. 2012b,a; Kannappan et al. 2013), and this is especially true for the faintest systems in the Local Group (as summarized in McConnachie 2012). A more realistic investigation of the HI content of Local Group galaxies is reserved for future work.

We further assume that any halo that has been within the virial radius of a giant has had all of its HI gas removed. This presupposes that a process such as ram pressure stripping removes the gas from satellites upon infall and is motivated by observations demonstrating that the vast majority of Local Group satellites have negligible neutral gas content (Greivich & Putman 2009). The small number of gas-poor dwarfs that lie beyond the virial radii of either M31 or the MW (i.e. Cetus and Tucana) may very well be explained as backslash halos (see Sales et al. 2007; Teyssier et al. 2012). Of course, some of the largest satellite galaxies in the LG (e.g. the LMC and NGC 205) are clearly able to retain HI for a non-negligible period of time after infall. This would suggest that our assumptions will lead to some under-counting of HI-rich galaxies, primarily at the highest masses.

The predicted HI mass functions within our simulated Local Volumes are plotted in Figure 12. The two systems with large interlopers have again been removed, and the line indicating Zeus & Hera is again plotted in magenta. The local HI mass function agrees well with predictions from

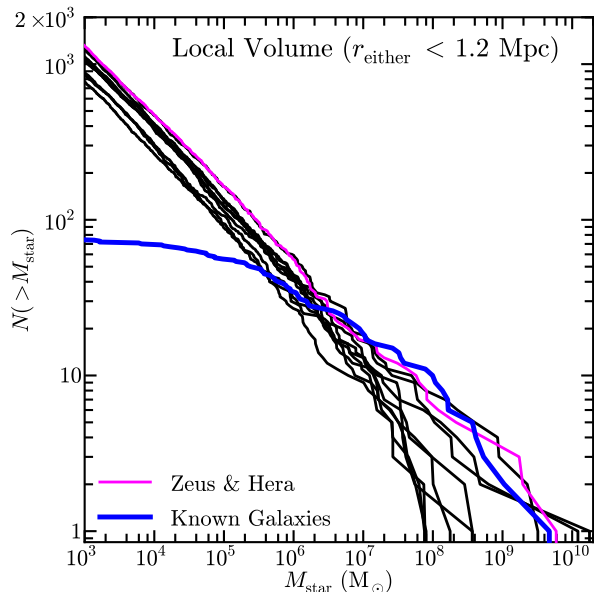


Figure 11. Cumulative stellar mass functions around paired hosts within the Local Volume using the preferred AM relation discussed in the text; not shown are those systems that include a third massive halo nearby (Siegfried & Roy and Serena & Venus). The pair Zeus & Hera are highlighted in magenta. The current count of galaxies within the same volume around the MW and M31 is shown in blue (McConnachie 2012), which flattens at small mass, likely because of incompleteness. We predict ~ 1000 galaxies having $M_* \geq 10^3 M_\odot$ within this volume, compared to the ~ 70 currently known.

ELVIS for $M_{\text{HI}} \gtrsim 5 \times 10^6 M_\odot$, at which point the local data break sharply, likely indicating incompleteness. We estimate that there are as many as ~ 50 (~ 300) unidentified galaxies with $M_{\text{HI}} \gtrsim 10^5 M_\odot$ ($10^3 M_\odot$) within 1.2 Mpc of the MW or M31.

4.3 Compact High Velocity Clouds as Minihalos

It is possible that some of these gas-rich objects have already been detected. Recently, Adams, Giovanelli, & Haynes (2013) presented a catalog of ultra-compact high velocity clouds (UCVHCs) extracted from the ALFALFA survey (Giovanelli et al. 2005; Haynes et al. 2011) and discussed the possibility that some of these objects may be dwarf galaxies (see also Blitz et al. 1999; Faerman et al. 2013). Adams et al. (2013) present 53 candidates, with HI properties that correspond to sizes of ~ 3 kpc and masses of $M_{\text{HI}} \simeq 10^5 - 10^6 M_\odot$ if they reside at ~ 1 Mpc distances. These characteristics are suggestively similar to those of known LG galaxies like Leo T. The ELVIS suite can be used to test whether these UCHVCs have properties (radial velocities and overall counts) that are consistent with those expected in Λ CDM for small halos in the Local Volume.

From Figure 12, we can immediately see that it is unlikely that *all* of the Adams et al. (2013) candidates are associated with small dark matter halos in the Local Volume. We expect fewer than 100 undiscovered objects *over the whole sky* with $M_{\text{HI}} \gtrsim 10^5 M_\odot$ within 1.2 Mpc of either host, while

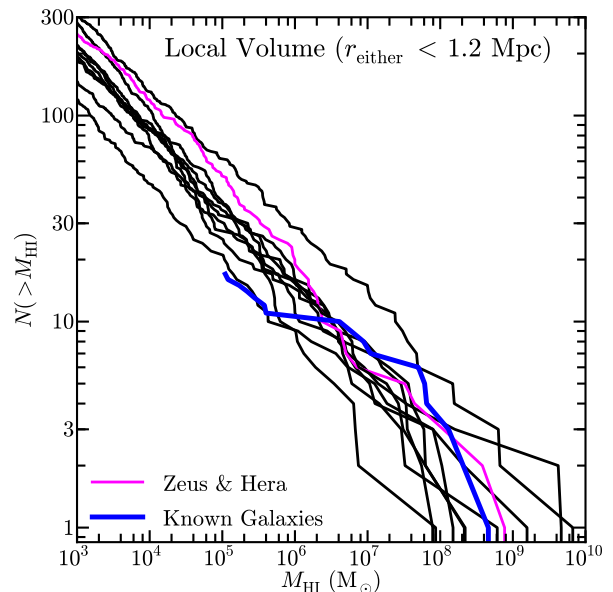


Figure 12. The HI mass functions within our simulated Local Volumes, excluding the systems with a third large host nearby. We assign gas masses via Equation 5, assuming that any halos that have passed within the virial radius of either giant since $z = 5$ have been stripped of all gas. The local HI mass function is consistent for $M_{\text{HI}} \gtrsim 5 \times 10^6 M_\odot$; below this value, incompleteness likely sets in. We expect perhaps ~ 50 undiscovered galaxies with $M_{\text{HI}} \geq 10^5 M_\odot$ within 1.2 Mpc of either host.

the ALFALFA sample has 53 candidates over only $\sim 10\%$ of the sky. Nevertheless, it would not be surprising if some of the identified candidates are indeed associated with dark-matter-dominated dwarfs.

The observed radial velocities of these clouds may provide clues for selecting the best candidates for follow-up. Figure 13 shows the normalized stacked radial velocity distribution of $M_{\text{HI}} > 10^5 M_\odot$ halos that sit between R_v and 1 Mpc (black curve), and between 1 and 2 Mpc (grey curve) of our ELVIS pairs, measured from the center of each host. We again exclude those objects with a third nearby giant from the black curve, and include only those objects with $R_{\text{res}} > 1.75$ Mpc (Zeus, Charybdis, Romulus, and Kek) in the grey curve, so as to minimize the effects of contamination from low resolution particles. The green curve shows the radial velocity distribution of candidate mini-halos from the Adams et al. (2013) UCHVC sample. It is important to recognize that the UCHVC sample is biased to avoid the region near $V_{\text{rad}} \approx 0 \text{ km s}^{-1}$ by construction. Nevertheless, the high-velocity tail of distribution shows some interesting differences compared to the predicted distribution.

The most important distinction between the simulated halos and the candidate objects is that there is a substantial population of UCHVCs with $175 \text{ km s}^{-1} \lesssim V_{\text{rad}} \lesssim 350 \text{ km s}^{-1}$. There are very few halos predicted with such high recessional velocities within 1 Mpc, and only slightly more out to 2 Mpc. We conclude that the sub-population of UCHVCs with these high velocities is unlikely to be associated with dark matter halos unless they are substantially more distant than 2 Mpc (in which

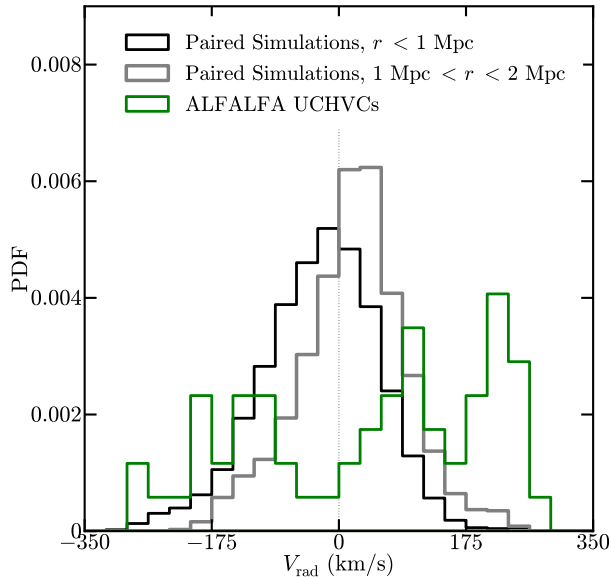


Figure 13. The black (grey) lines show the normalized radial velocity distribution of all predicted galaxies with $M_{\text{HI}} > 10^5 M_{\odot}$ within 1 Mpc (2 Mpc) of each host. The green line shows the radial velocities of the UCHVC halo candidates from Adams et al. (2013). While a selection bias limits the abundance of UCHVCs with $V_{\text{rad}} \sim 0 \text{ km s}^{-1}$, the differences at the high radial velocity tail is illuminating. Specifically, UCHVCs with $V_{\text{rad}} > 175 \text{ km s}^{-1}$ are highly unlikely to be associated with small halos in the Local Volume according to our predictions. Systems with lower radial velocities are likely better candidates for follow up.

case their total gas mass would become very large and thus the expected count would drop considerably). Based on these results, we suggest that targeted follow-up searches for nearby mini-halos may want to focus on UCHVC candidates with $V_{\text{rad}} \lesssim 150 \text{ km s}^{-1}$.

We also compare the on-the-sky positions of the possible minihalos around the Milky Way to those of the gas rich objects near Hera, the host that we have highlighted throughout this work, in a Hammer projection in Figure 14. The diamonds indicate the predicted galaxies around Hera and the circles denote the minihalo candidates from ALFALFA; both are colored by their relative radial velocities according to the color bar. We have oriented the coordinate system such that Hera’s partner halo Zeus sits at the (l, b) of M31 (indicated by the star). The grey crosses are back-splash halos. There is a clear clustering of back-splash objects near Zeus and a corresponding dearth of gas-rich halos. Suggestively, the receding ALFALFA objects, which seem most inconsistent with the velocity distributions in ELVIS, are located near one another. We do note, however, that the gas clouds identified by ALFALFA may instead be more distant objects that are perhaps still a part of the Hubble Flow. We find that most objects more than 1.5 Mpc from the center of each host are receding.

4.4 The Local Hubble Relation

The velocity field within the Local Volume contains a wealth of information on the assembly history and mass of the Local Group (Kahn & Woltjer 1959; Karachentsev et al. 2002; Karachentsev 2005; Peirani & de Freitas Pacheco 2006; Teyssier et al. 2012; van der Marel et al. 2012). The ELVIS simulations supply a potentially valuable basis for interpreting these data, and we intend to utilize them for this purpose in future work. Here we briefly examine the local velocity-distance relation in one of our simulations in order to demonstrate broad agreement with data and illustrate the potential for a more in-depth interpretive analysis.

Figure 15 shows the local Hubble relation centered on the Local-Group barycenter along with data from the Zeus & Hera simulation. MW and M31 are indicated as red and blue squares, respectively, calculated from the separation and radial velocity given in Table 1 and the masses in Table 2. Known Local Group galaxies that reside beyond 300 kpc of either giant are shown as large diamonds; the two highlighted in yellow are the gas-free dwarfs Cetus and Tucana, which are back-splash candidates. The Leo P data point is calculated from Tables 1 and 2, assuming that its distance from the MW is 1.75 Mpc (McQuinn et al. 2013); the remainder of the observational data is taken from McConnachie (2012). For comparison, circles show all halos within the Zeus & Hera simulation that are large enough, according to our preferred abundance matching relation, to have stellar masses exceeding $3000 M_{\odot}$. Halos within 300 kpc of either simulated giant are excluded, but galaxies that have been within the virial radii of Zeus or Hera are colored blue and red, respectively.

As expected from the previous discussion (e.g. Figure 8), back-splash halos tend to populate the outflowing, positive-velocity envelope of the relation. The gas-free dwarfs Cetus and Tucana are similarly consistent with inhabiting this upper envelope. More generally, the simulated relation is a reasonably good match to the data shown. The relative lack of known galaxies with $V_r \lesssim -100 \text{ km s}^{-1}$ is likely related to the barycentric velocities of the MW and M31, which are moving $\sim 50 \text{ km s}^{-1}$ slower than Zeus and Hera.

Finally, we note that the vertical dashed line near 1.75 Mpc in Figure 15 indicates the position of the first low-resolution (contamination) particle in the simulation. In principle, our predictions could be compromised beyond this point, but based on larger (lower resolution) simulation comparisons we find no evidence that contamination biases bulk velocity predictions.

5 CONCLUSIONS

This work presents the ELVIS suite, a set of collisionless cosmological simulations consisting of twelve Local Group-like pairs of MW/M31-size dark matter halos and twenty-four isolated analogs mass-matched to those in the pairs. Each simulation resolves mini-halos down to $M_{\text{peak}} = 6 \times 10^7 M_{\odot}$ within high-resolution, contamination-free volumes that span 2 to 5 Mpc in size.

One of the goals of this work is to determine if the Milky Way and M31 are expected to be biased in any way

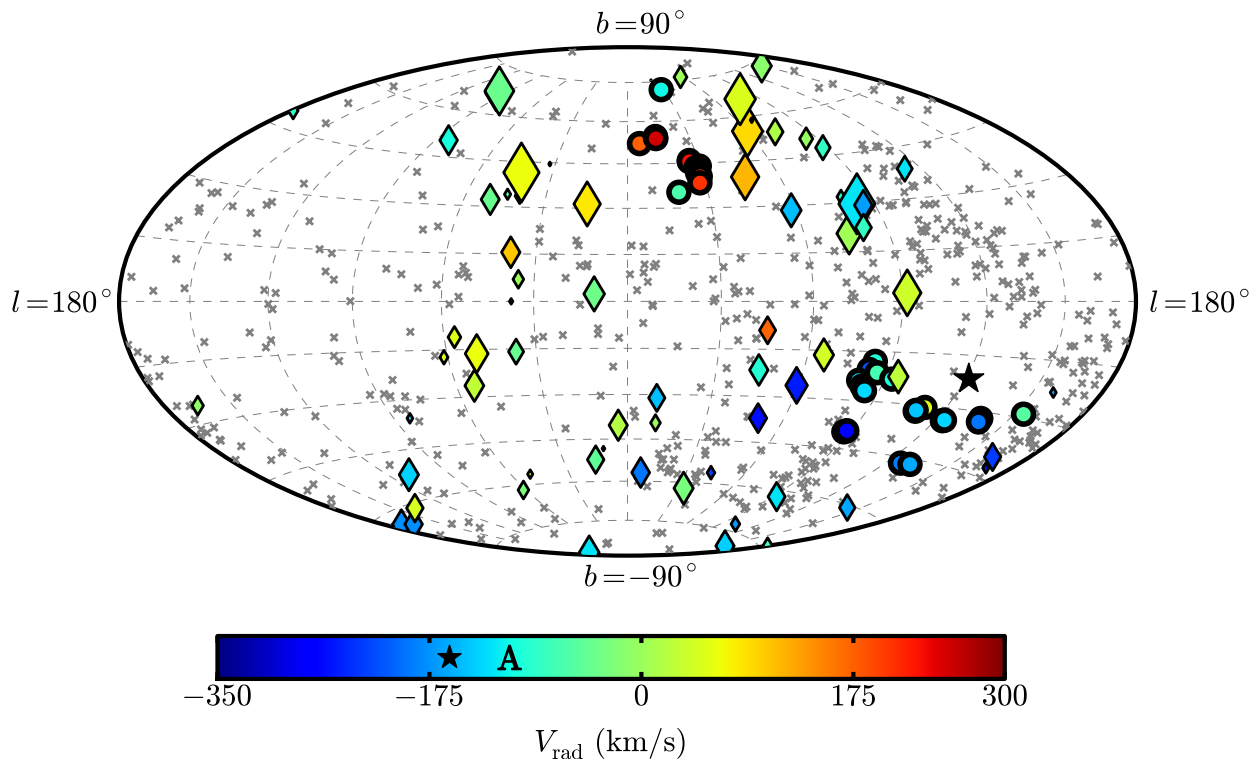


Figure 14. A Hammer projection of the halos within 1 Mpc of Hera in mock Galactic coordinates, highlighting the halos we expect to be gas rich with diamonds and marking backplash halos with crosses; no subhalos of either giant are plotted. The simulation is rotated such that Zeus and M31 lie in the same position on the sky; this point is marked with a star. The size of the diamonds is proportional to our modeled gas mass values and distances as $\log(M_{\text{HI}}/r^2)$. The UCHVC minihalo candidates from Adams et al. (2013) are plotted as circles with thick outlines. These and the gas rich objects are colored by their radial velocities according to the color bar; the approach velocities of Zeus and Andromeda are indicated on the color bar by the star and the A, respectively. The velocities of the fastest (outflowing) UCHVCs in the north are clearly outliers compared to the expected velocities of halos in this region and therefore may be poor candidates for follow-up to discover dwarf galaxies. The infalling systems in the south are more in line with our kinematic expectations for mini-halos.

with respect to typical field halos as a result of their paired configuration. We find no evidence that this is the case (c.f. Figure 3). Statistically, subhalo properties (counts and kinematics) and host halo properties (formation times and concentrations) are indistinguishable between our paired and unpaired samples. We provided analytic fits to subhalo mass functions in § 3.1 (and for V_{max} functions in Appendix B). Apparently, as long as measures are restricted to the virial volumes, simulated field halos provide an adequate comparison set for the Milky Way and M31.

As might be expected, differences become more apparent between paired and isolated samples when we explore measures beyond the virial volumes of either hosts (Figures 4–6). The Local Volume at 1.2 Mpc distance around each paired host contains, on average, 80% more halos at fixed M_{peak} than the corresponding region surrounding each isolated host. Similarly, the kinematic properties of the minihalo population around Local Group-like pairs show distinct differences from isolated MWs: the tangential velocity distributions for halos around pairs are significantly hotter, and the radial velocity distributions are skewed towards more outflowing systems. The tendency to see more outwardly

moving halos around paired hosts is likely related to another difference we see: an increase in the backplash fraction. We find evidence that paired halos have an increased fraction of satellite systems that are now beyond the virial radius of either host, but that had previously been inside (Figure 7). These backplash objects are preferentially moving outward along more radial orbits at $z = 0$ (Figure 8).

With these basic comparisons in place, we investigate our sample of LG-like pairs more closely, focusing on comparisons with data throughout the Local Volume. A summary of the resultant work is as follows:

- We find that the abundance matching relation presented by Behroozi et al. (2013c) over-predicts the number of $M_{\star} \sim 5 \times 10^6 M_{\odot}$ satellites within 300 kpc of the MW and M31 (Figure 10), a regime where the satellite census is believed to be complete.
- We present a modified Behroozi relation, motivated by the stellar mass function reported by Baldry et al. (2012) from GAMA data (Figure 9 and Equation 4), that reproduces the observed satellite count down to $M_{\star} \sim 5 \times 10^5 M_{\odot}$, a point where incompleteness likely becomes an issue. It

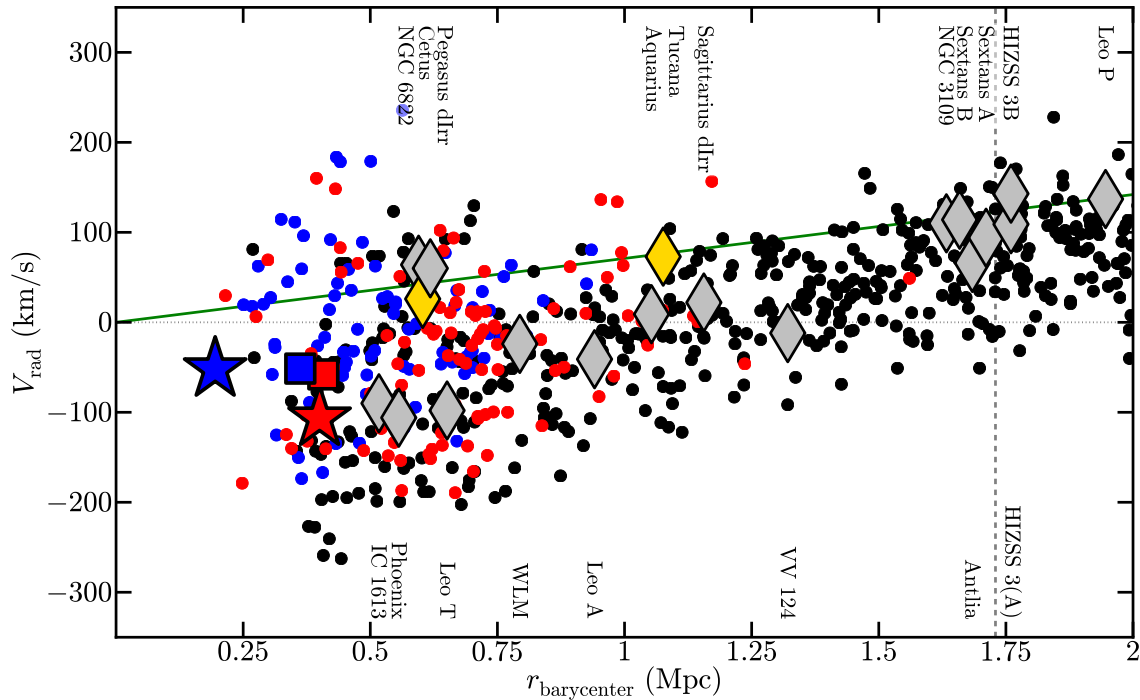


Figure 15. Barycentric radial velocity vs. barycentric distance for Local Group galaxies compared to expectations from the Zeus & Hera simulation. The centers of Zeus (blue) and Hera (red) are indicated by large stars, while M31 (blue) and the MW (red) are shown by squares. All halos with $M_\star > 3 \times 10^3 M_\odot$ and beyond 300 kpc of either Zeus or Hera are plotted as circles. Large diamonds indicate known galaxies in the Local Group beyond 300 kpc of either giant. Backsplash halos of Zeus are shown as blue while those that have interacted with Hera are plotted in red. The black points are halos that have yet to be accreted by either host. The grey diamonds mark LG galaxies that have gas while the yellow diamonds correspond to Cetus and Tucana, two gas-free dwarf that are good backslash candidates. For reference, the green line shows the asymptotic linear Hubble relation for our simulated cosmology.

also reproduces galaxy counts throughout the Local Volume down to $M_\star \sim 5 \times 10^6 M_\odot$, below which incompleteness is almost certainly an issue (Figure 11).

- By extrapolating our preferred abundance matching relation to low halo masses, we find there should be ~ 300 galaxies with $M_\star \geq 10^3 M_\odot$ within 300 kpc of the Milky Way and ~ 1000 such galaxies within 1.2 Mpc of either host. LSST (along with ongoing surveys) will test this expectation. If faint galaxies are not discovered in large numbers, it could point to a break in the stellar-mass to halo-mass relation at the low-mass end.

- Using empirical relations between HI mass and stellar mass, we predict the number of gas-rich galaxies within the Local Volume (Figure 12). The observed LG HI mass function agrees well with our expectations down to $M_{\text{HI}} \sim 10^7 M_\odot$, below which the data may suffer from incompleteness. We conclude that there may be approximately 50 undiscovered gas-rich halos with $M_{\text{HI}} > 10^5 M_\odot$ within 1.2 Mpc of the Milky Way and M31.

- We compare the properties of our modeled gas-rich halos to the UCHVC mini-halo candidates presented by ALFALFA (Adams et al. 2013, Figures 13 and 14). While the characteristics of many of these clouds make them good candidates for gas-rich halos, it is highly unlikely that more than $\sim 10\%$ are true mini-halos. In particular, positive radial velocities in excess of 175 km s^{-1} are drastically inconsistent

with our expectations for halo kinematics within ~ 2 Mpc of the MW.

Our results generally indicate that studies focusing on basic properties within the virial volumes of the MW or M31 can be fairly compared to predictions from more isolated field-halo simulations (e.g. Diemand et al. 2008; Kuhlen et al. 2008; Springel et al. 2008). However, simulations investigating the volume surrounding the Milky Way *must* account for the overall environment that it lives in – specifically, the presence of the approaching M31 galaxy.

Acknowledgments

Support for this work was provided by NASA through a *Hubble Space Telescope* theory grant (program AR-12836) from the Space Telescope Science Institute (STScI), which is operated by the Association of Universities for Research in Astronomy (AURA), Inc., under NASA contract NAS5-26555. This work was also funded in part by NSF grants AST-1009999, AST-1009973, and NASA grant NNX09AD09G. M.B.-K. acknowledges support from the Southern California Center for Galaxy Evolution, a multi-

campus research program funded by the University of California Office of Research. J.S.B. was partially supported by the Miller Institute for Basic Research in Science during a Visiting Miller Professorship in the Department of Astronomy at the University of California Berkeley.

The authors thank Frank van den Bosch, Michael Cooper, Manoj Kaplinghat, Evan Kirby, Jose Oñorbe, Julio Navarro, Annika Peter, and Risa Wechsler for helpful comments, and Erik Tollerud for aid in creating the visualizations. We also thank Volker Springel for making *Gadget-2* publicly available and for providing a version of *Gadget-3* for our use, Peter Behroozi for making *Rockstar* and *consistent-trees* publicly available, and Oliver Hahn for making *MUSIC* publicly available. Finally, we gratefully acknowledge the computational support of the NASA Advanced Supercomputing Division and the NASA Center for Climate Simulation, upon whose *Pleiades* and *Discover* systems these simulations were run, and the *Greenplanet* cluster at UCI, upon which much of the secondary analysis was performed.

APPENDIX A: NUMERICAL CONVERGENCE

In this Appendix, we compare the M_{peak} and V_{max} functions within 400 kpc of iKauket at three different levels of numerical resolution. Figure 16 contains this comparison: results from the HiRes simulation ($m_p = 2.35 \times 10^4 M_{\odot}$, $\epsilon = 70.4$ pc) are shown as a red dashed line, while results from the run at our fiducial resolution ($m_p = 1.89 \times 10^5 M_{\odot}$, $\epsilon = 141$ pc) are shown as a solid black line. For comparison, the blue line shows a lower resolution run as well ($m_p = 1.55 \times 10^6 M_{\odot}$, $\epsilon = 469$ pc).

The left panel plots the number of halos identified by our pipeline with M_{peak} greater than a given mass; on the right, we plot the current V_{max} function. By locating where our fiducial resolution begins to systematically differ from the HiRes run, it is clear that halos with $V_{\text{max}} > 8$ km/s and $M_{\text{peak}} > 6 \times 10^7 M_{\odot}$ are reliably identified at the fiducial resolution. These resolution limits are marked by dashed vertical lines in the plots.

APPENDIX B: V_{max} FUNCTIONS

For most galaxies, it is more convenient to measure circular velocities or velocity dispersions than virial mass. Although we do show stellar mass functions in the main body, our relation is not a mapping between M_{\star} and V_{max} ; thus, we show V_{max} functions for direct comparison with such observations here. As with the M_{peak} functions, counts as a function of V_{max} agree well within R_v , and are both well fit by a power law at the low mass end:

$$N_v(> V_{\text{max}}/V_v) = 0.038(V_{\text{max}}/V_v)^{-3.3}.$$

The V_{max} function in the Local Fields are also similarly offset, with the paired simulations lying 75% higher than the isolated analogs:

$$N_{0.3-1}(> V_{\text{max}}) = N_0 \left(\frac{V_{\text{max}}}{10 \text{ km/s}} \right)^{-3.1},$$

with $N_0 = 540$ for the paired sample and 300 for the isolated analogs. Likewise, we predict similar numbers of objects with

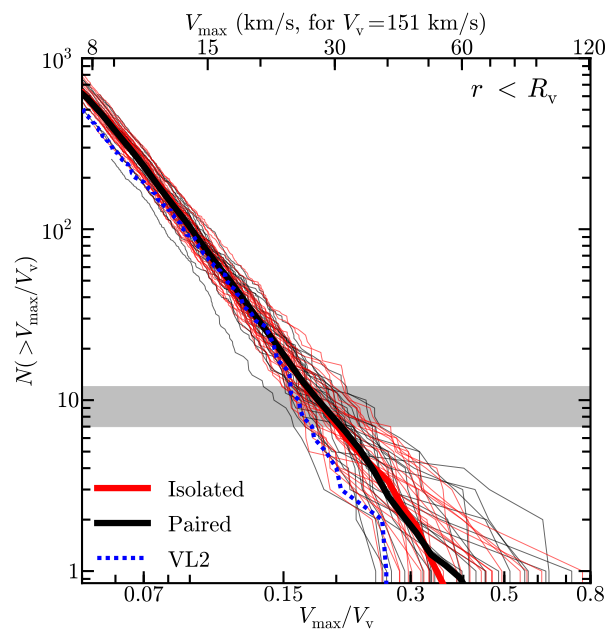


Figure 17. The V_{max} function within R_v of each host, scaled by the virial velocity of that host, analogous to Figure 3. As in that Figure, the two populations agree well within the virial radius and are both well fit at the low-mass end by a power law of slope -3.1 , as given in the text. The blue dashed line plots the V_{max} function within the virial radius of the high-resolution Via Lactea II halo (Kuhlen et al. 2009), which agrees within the halo-to-halo scatter.

$V_{\text{max}} > 8 \text{ km s}^{-1}$ within the 1 Mpc of each host and within the Local Volume around each pair as predicted in Figure 5 for $M_{\text{peak}} > 6 \times 10^7 M_{\odot}$; these V_{max} functions are plotted in Figure 19.

References

- Adams E. A. K., Giovanelli R., Haynes M. P., 2013, arXiv:1303.6967 [astro-ph]
 Arraki K. S., Klypin A., More S., Trujillo-Gomez S., 2012, arXiv:1212.6651 [astro-ph]
 Baldry I. K. et al., 2012, MNRAS, 421, 621
 Baldry I. K., Glazebrook K., Driver S. P., 2008, MNRAS, 388, 945
 Behroozi P. S., Wechsler R. H., Conroy C., 2013c, ApJ, 770, 57
 Behroozi P. S., Wechsler R. H., Wu H.-Y., 2013a, ApJ, 762, 109
 Behroozi P. S., Wechsler R. H., Wu H.-Y., Busha M. T., Klypin A. A., Primack J. R., 2013b, ApJ, 763, 18
 Blitz L., Robishaw T., 2000, ApJ, 541, 675
 Blitz L., Spergel D. N., Teuben P. J., Hartmann D., Burton W. B., 1999, ApJ, 514, 818
 Boselli A., Boissier S., Cortese L., Gavazzi G., 2008, ApJ, 674, 742
 Bovy J., Rix H.-W., 2013, arXiv:1309.0809 [astro-ph]
 Boylan-Kolchin M., Bullock J. S., Kaplinghat M., 2011, MNRAS, 415, L40
 Boylan-Kolchin M., Bullock J. S., Kaplinghat M., 2012, MNRAS, 422, 1203

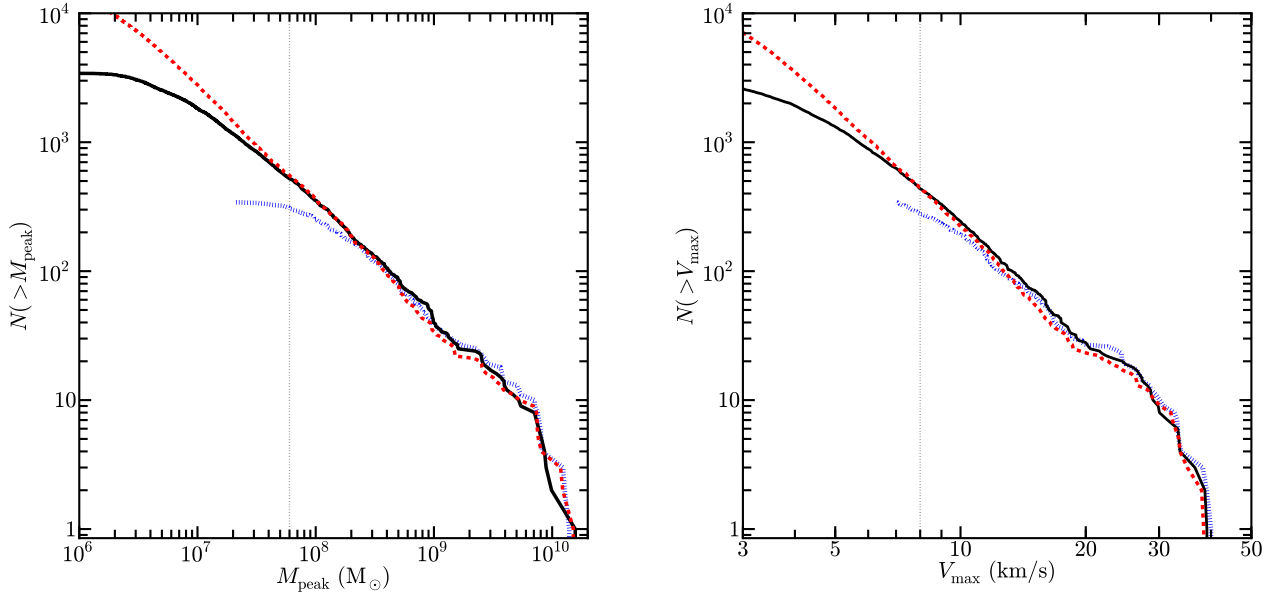


Figure 16. Resolution test indicating the smallest halos *Rockstar* reliably identifies in the ELVIS simulations. Here we plot the M_{peak} (left) and V_{max} (right) functions for halos within 400 kpc of the smallest of our isolated halos, iKauket. The black line indicates the fiducial resolution; the red line is from the HiRes simulation, and the blue line is from a lower resolution run, for illustrative purposes. The mass and circular velocity at which the lines begin to systematically disagree, $M_{\text{peak}} = 6 \times 10^7 M_{\odot}$ and $V_{\text{max}} = 8 \text{ km s}^{-1}$, constitute our resolution limits for the fiducial resolution.

- Boylan-Kolchin M., Bullock J. S., Sohn S. T., Besla G., van der Marel R. P., 2013, *ApJ*, 768, 140
- Boylan-Kolchin M., Springel V., White S. D. M., Jenkins A., 2010, *MNRAS*, 406, 896
- Boylan-Kolchin M., Springel V., White S. D. M., Jenkins A., Lemson G., 2009, *MNRAS*, 398, 1150
- Bryan G. L., Norman M. L., 1998, *ApJ*, 495, 80
- Bullock J. S., Kolatt T. S., Sigad Y., Somerville R. S., Kravtsov A. V., Klypin A. A., Primack J. R., Dekel A., 2001, *MNRAS*, 321, 559
- Bullock J. S., Kravtsov A. V., Weinberg D. H., 2000, *ApJ*, 539, 517
- Busha M. T., Wechsler R. H., Behroozi P. S., Gerke B. F., Klypin A. A., Primack J. R., 2011, *ApJ*, 743, 117
- Conroy C., Wechsler R. H., Kravtsov A. V., 2006, *ApJ*, 647, 201
- Corbelli E., 2003, *MNRAS*, 342, 199
- Davis M., Efstathiou G., Frenk C. S., White S. D. M., 1985, *ApJ*, 292, 371
- Diemand J., Kuhlen M., Madau P., 2007a, *ApJ*, 657, 262
- Diemand J., Kuhlen M., Madau P., 2007b, *ApJ*, 667, 859
- Diemand J., Kuhlen M., Madau P., Zemp M., Moore B., Potter D., Stadel J., 2008, *Nature*, 454, 735
- Driver S. P. et al., 2011, *MNRAS*, 413, 971
- Faerman Y., Sternberg A., McKee C. F., 2013, arXiv:1309.0815 [astro-ph]
- Fardal M. A. et al., 2013, arXiv:1307.3219 [astro-ph]
- Few C. G., Gibson B. K., Courty S., Michel-Dansac L., Brook C. B., Stinson G. S., 2012, *A&A*, 547, A63
- Forero-Romero J. E., Hoffman Y., Bustamante S., Gottlöber S., Yepes G., 2013, *ApJ*, 767, L5
- Forero-Romero J. E., Hoffman Y., Yepes G., Gottlöber S., Piontek R., Klypin A., Steinmetz M., 2011, *MNRAS*, 417, 1434
- Garrison-Kimmel S., Rocha M., Boylan-Kolchin M., Bullock J. S., Lally J., 2013, *MNRAS*
- Gill S. P. D., Knebe A., Gibson B. K., 2005, *MNRAS*, 356, 1327
- Giovanelli R. et al., 2013, arXiv:1305.0272 [astro-ph]
- Giovanelli R. et al., 2005, *AJ*, 130, 2598
- Gottlöber S., Hoffman Y., Yepes G., 2010, arXiv:1005.2687 [astro-ph]
- Grcevich J., Putman M. E., 2009, *ApJ*, 696, 385
- Gross M. A. K., Somerville R. S., Primack J. R., Holtzman J., Klypin A., 1998, *MNRAS*, 301, 81
- Hahn O., Abel T., 2011, *MNRAS*, 415, 2101
- Haynes M. P. et al., 2011, *AJ*, 142, 170
- Huang S., Haynes M. P., Giovanelli R., Brinchmann J., 2012b, *ApJ*, 756, 113
- Huang S., Haynes M. P., Giovanelli R., Brinchmann J., Stierwalt S., Neff S. G., 2012a, *AJ*, 143, 133
- Ivezic Z. et al., 2008, arXiv:0805.2366 [astro-ph]
- Jenkins A., Frenk C. S., White S. D. M., Colberg J. M., Cole S., Evrard A. E., Couchman H. M. P., Yoshida N., 2001, *MNRAS*, 321, 372
- Kahn F. D., Woltjer L., 1959, *ApJ*, 130, 705
- Kannappan S. J., 2004, *ApJ*, 611, L89
- Kannappan S. J. et al., 2013, arXiv:1308.3292 [astro-ph]
- Karachentsev I. D., 2005, *AJ*, 129, 178
- Karachentsev I. D., Kaisina E. I., 2013, *AJ*, 146, 46
- Karachentsev I. D., Karachentseva V. E., Huchtmeier W. K., Makarov D. I., 2004, *AJ*, 127, 2031
- Karachentsev I. D. et al., 2002, *A&A*, 389, 812
- Katz N., White S. D. M., 1993, *ApJ*, 412, 455

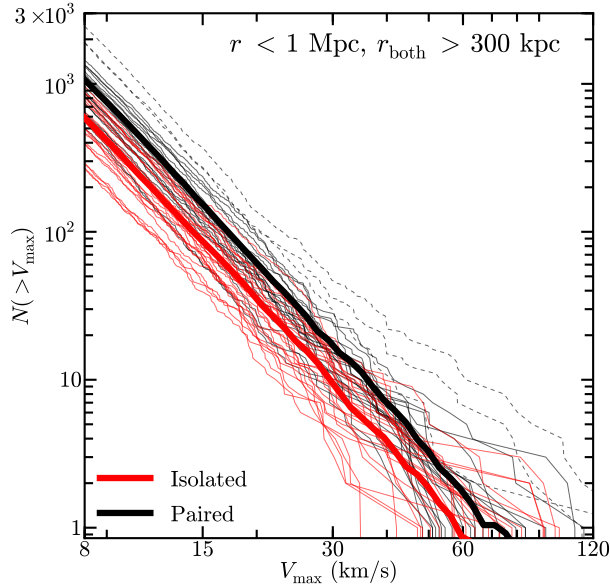


Figure 18. The V_{\max} functions for objects in the Local Field (within 1 Mpc of the host, but more than 300 pc from both giants). The average relations are offset from one another, with the paired simulations having an amplitude that is 75% higher. The power law fits to the average relations are given in the text.

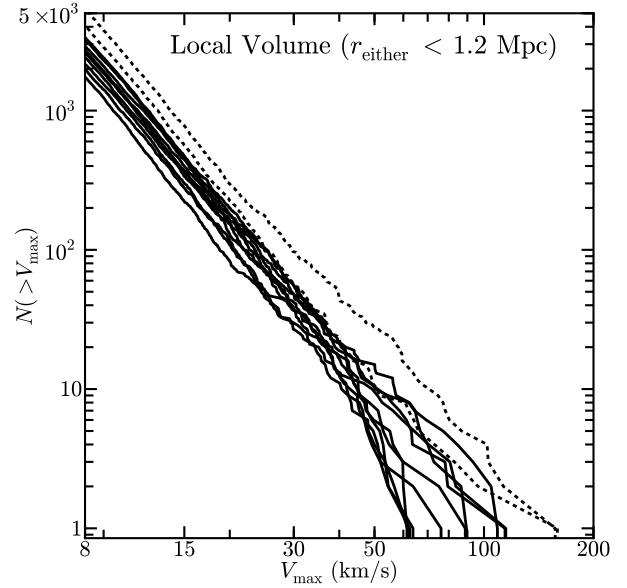


Figure 19. The V_{\max} functions in the Local Volume (1.2 Mpc of either host), analogous to Figure 5.

Kawata D., Mulchaey J. S., 2008, *ApJ*, 672, L103
 Kazantzidis S., Mayer L., Mastropietro C., Diemand J., Stadel J., Moore B., 2004, *ApJ*, 608, 663
 Klypin A., Kravtsov A. V., Valenzuela O., Prada F., 1999, *ApJ*, 522, 82
 Klypin A. A., Trujillo-Gomez S., Primack J., 2011, *ApJ*, 740, 102
 Knollmann S. R., Knebe A., 2009, *ApJS*, 182, 608
 Koposov S. et al., 2008, *ApJ*, 686, 279
 Koposov S. E., Yoo J., Rix H., Weinberg D. H., Macciò A. V., Escudé J. M., 2009, *ApJ*, 696, 2179
 Kravtsov A. V., Berlind A. A., Wechsler R. H., Klypin A. A., Gottlöber S., Allgood B., Primack J. R., 2004, *ApJ*, 609, 35
 Kuhlen M., Diemand J., Madau P., 2008, *ApJ*, 686, 262
 Kuhlen M., Madau P., Silk J., 2009, *Science*, 325, 970
 Larson D. et al., 2011, *ApJS*, 192, 16
 Li Y.-S., White S. D. M., 2008, *MNRAS*, 384, 1459
 Libeskind N. I., Yepes G., Knebe A., Gottlöber S., Hoffman Y., Knollmann S. R., 2010, *MNRAS*, 401, 1889
 Madau P., Kuhlen M., Diemand J., Moore B., Zemp M., Potter D., Stadel J., 2008, *ApJ*, 689, L41
 Makarov D., Karachentsev I., 2011, *MNRAS*, 412, 2498
 Mamon G. A., Sanchis T., Salvador-Solé E., Solanes J. M., 2004, *A&A*, 414, 445
 McConnachie A. W., 2012, *AJ*, 144, 4
 McConnachie A. W., Irwin M. J., Ferguson A. M. N., Ibata R. A., Lewis G. F., Tanvir N., 2005, *MNRAS*, 356, 979
 McGaugh S. S., 2005, *ApJ*, 632, 859
 McQuinn K. B. W. et al., 2013, arXiv:1310.0044 [astro-ph]
 Miller R. H., 1964, *ApJ*, 140, 250
 Moore B., Ghigna S., Governato F., Lake G., Quinn T.,

Stadel J., Tozzi P., 1999, *ApJ*, 524, L19
 Moster B. P., Naab T., White S. D. M., 2013, *MNRAS*, 428, 3121
 Navarro J. F., Frenk C. S., White S. D. M., 1996, *ApJ*, 462, 563
 Oñorbe J., Garrison-Kimmel S., Maller A. H., Bullock J. S., Rocha M., Hahn O., 2013, arXiv:1305.6923 [astro-ph]
 Olsen K. A. G., Zaritsky D., Blum R. D., Boyer M. L., Gordon K. D., 2011, *ApJ*, 737, 29
 Peirani S., de Freitas Pacheco J. A., 2006, *New Astronomy*, 11, 325
 Phillips J. I., Wheeler C., Boylan-Kolchin M., Bullock J. S., Cooper M. C., Tollerud E. J., 2013, arXiv:1307.3552 [astro-ph]
 Piffi T. et al., 2013, arXiv:1309.4293 [astro-ph]
 Rhode K. L. et al., 2013, *AJ*, 145, 149
 Richardson J. C. et al., 2011, *ApJ*, 732, 76
 Ricotti M., Gnedin N. Y., 2005, *ApJ*, 629, 259
 Rocha M., Peter A. H. G., Bullock J., 2012, *MNRAS*, 425, 231
 Ryan-Weber E. V., Begum A., Oosterloo T., Pal S., Irwin M. J., Belokurov V., Evans N. W., Zucker D. B., 2008, *MNRAS*, 384, 535
 Sales L. V., Navarro J. F., Abadi M. G., Steinmetz M., 2007, *MNRAS*, 379, 1475
 Springel V., 2005, *MNRAS*, 364, 1105
 Springel V. et al., 2008, *MNRAS*, 391, 1685
 Springel V. et al., 2005, *Nature*, 435, 629
 Sternberg A., McKee C. F., Wolfire M. G., 2002, *ApJS*, 143, 419
 Stewart K. R., Bullock J. S., Wechsler R. H., Maller A. H., 2009, *ApJ*, 702, 307
 Strigari L. E., Bullock J. S., Kaplinghat M., Simon J. D., Geha M., Willman B., Walker M. G., 2008, *Nature*, 454, 1096

- Strigari L. E., Frenk C. S., White S. D. M., 2010, MNRAS, 408, 2364
- Teyssier M., Johnston K. V., Kuhlen M., 2012, MNRAS, 426, 1808
- Tikhonov A. V., Klypin A., 2009, MNRAS, 395, 1915
- Tollerud E. J., Barton E. J., Bullock J. S., Trinh C., 2011, in EAS Publications Series, Vol. 48, EAS Publications Series, Koleva M., Prugniel P., Vauglin L., eds., pp. 455–457
- Tollerud E. J. et al., 2012, ApJ, 752, 45
- Tollerud E. J., Bullock J. S., Strigari L. E., Willman B., 2008, ApJ, 688, 277
- Tully R. B. et al., 2013, AJ, 146, 86
- Vale A., Ostriker J. P., 2004, MNRAS, 353, 189
- van der Marel R. P., Fardal M., Besla G., Beaton R. L., Sohn S. T., Anderson J., Brown T., Guhathakurta P., 2012, ApJ, 753, 8
- Walker M. G., Peñarrubia J., 2011, ApJ, 742, 20
- Weisz D. R. et al., 2011, ApJ, 743, 8
- Woo J., Courteau S., Dekel A., 2008, MNRAS, 390, 1453
- Woo J. et al., 2013, MNRAS, 428, 3306
- Wu H.-Y., Hahn O., Wechsler R. H., Behroozi P. S., Mao Y.-Y., 2013, ApJ, 767, 23
- Yniguez B., Garrison-Kimmel S., Boylan-Kolchin M., Bullock J. S., 2013, arXiv:1305.0560 [astro-ph]
- Zentner A. R., Bullock J. S., 2003, ApJ, 598, 49
- Zolotov A. et al., 2012, ApJ, 761, 71